ФИЗИКА ЭЛЕМЕНТАРНЫХ ЧАСТИЦ И АТОМНОГО ЯДРА
2012. Т. 43. ВЫП. 1

SOME TOP-QUARK PROPERTIES MEASURED IN $p\bar{p}$ COLLISIONS USING CDF DETECTOR AT $\sqrt{s} = 1.96$ TeV

V. B. Flyagin, V. V. Glagolev

Joint Institute for Nuclear Research, Dubna

ФИЗИКА ЭЛЕМЕНТАРНЫХ ЧАСТИЦ И АТОМНОГО ЯДРА
2012. Т. 43. ВЫП. 1

SOME TOP-QUARK PROPERTIES MEASURED IN $p\bar{p}$ COLLISIONS USING CDF DETECTOR AT $\sqrt{s} = 1.96$ TeV

V. B. Flyagin, V. V. Glagolev

Joint Institute for Nuclear Research, Dubna

This review considers important properties of the top quark. The top quark decays before hadronization, and the spin information is directly transferred to the decay products. Therefore, the structure of the weak interaction is investigated by measuring the helicity fractions, f, of the W boson — the top-quark decay product. Other investigations: search for the presence of $V + A$ interaction, search for exotic top-quark charge $-4/3$ and for $t\bar{t}$ resonances — all of them, so far, were not found in the experiments — testify against going out of the Standard Model.

В обзоре рассматриваются важные свойства топ-кварка. Топ-кварк распадается до адронизации, и информация о его спине передается непосредственно продуктам его распада. Поэтому структура слабого взаимодействия исследуется посредством измерения фракций спиральности, f, W-бозона — продукта распада топ-кварка. Другие исследования: поиск присутствия $V + A$-взаимодействия, поиск экзотического заряда топ-кварка $-4/3$ и $t\bar{t}$-резонансов (все они пока не найдены в экспериментах) — свидетельствуют против выхода за пределы Стандартной модели.

PACS: 29.20.db; 29.40.Gx; 29.40.Mc; 29.40.Vj; 29.40.Wk; 25.43.+t; 14.65.Ha

INTRODUCTION

Since the discovery of the top quark in 1995 by the CDF and DØ Collaborations [1, 2], the mass of this most massive known elementary particle has been measured with high precision. However, the measurements of other top-quark properties are still statistically limited, so the question remains whether the Standard Model (SM) successfully predicts these properties. At the Tevatron collider, with a center-of-mass energy of 1.96 TeV, most top quarks are pair-produced via the strong interaction. In the Standard Model, the top quark decays in nearly 100% of all cases into a W boson and a b quark. Due to its large mass (≈ 172 GeV) and a very short lifetime ($\approx 5 \cdot 10^{-25}$ s), that is shorter than the hadronization time ($\approx 10^{-23}$ s), the top quark exhibits a lot of unique features not observed for the lighter quarks. Its very short lifetime means that the top-quark spin characteristics are not diluted by hadronization. Thus its decay products preserve the helicity content of the underlying weak interaction. The large mass of the top

quark means that it is produced at very short distances and thus its production is characterized by a small coupling constant $\alpha_s(m_{\rm top}) \approx 0.1$, i.e., it is a very good perturbative object for testing of QCD. In addition, its Yukawa coupling is approximately 1. It suggests that the top quark can play an important role in the electroweak symmetry breaking. Anomalies in the $t\bar{t}$ production would indicate the presence of a new physics. The presence of anomalous couplings in the top-quark processes would modify the top-quark kinematic distributions (e.g., $t\bar{t}$ invariant mass). The forward–backward asymmetries in the top-pair production, different from those $t\bar{t}$ expected in the NLO of QCD, can also indicate a new physics. In general it can be said that top-quark physics is a window for looking for a new physics.

In this review the following topics are discussed:

The structure of the weak interaction is investigated by measuring the helicity fractions of the W boson in top-quark decays.

In the SM, the top quark is an upper quark of the third generation with the electric charge of $+2/3$. Because the top-quark electric charge is so far not measured, therefore one cannot exclude an alternative interpretation that is based on a conception of an exotic quark with charge $-4/3$. Below one of the first such measurements is presented.

In the end, we describe the search for exotic resonant $t\bar{t}$ production that would appear as unexpected structure in the spectrum of the invariant mass of $t\bar{t}$ pairs $M_{t\bar{t}}$. Previous searches using ≈ 100 pb^{-1} samples from Fermilab Tevatron Run I have ruled out any production of a narrow top color resonance with mass less than 480 GeV/c^2.

All the results confirm a good agreement between the data and SM.

1. MEASUREMENT OF W-BOSON HELICITY FRACTIONS IN TOP-QUARK DECAYS USING $\cos\theta^*$

This section is devoted to measurements of the W-boson helicity fractions by two different methods [4, 5] using data corresponding to an integrated luminosity of 1.9 fb^{-1} of $p\bar{p}$ collisions at a center-of-mass energy of 1.96 TeV collected by the CDF II detector operating at the Fermilab Tevatron. Combining the results obtained by these two methods, the authors have found a good consistence with the SM expectations.

Here is also presented the report [30] (Subsec. 1.6), where there has been measured an upper limit on the fraction of $V + A$ current, f_{V+A}, in the top-quark decays, using approximately 700 pb^{-1} at the same energy, using the decay $t \to Wb \to \ell\nu b$ (where $\ell = e$ or μ), which is sensitive to the polarization of the W boson. It was determined $f_{V+A} = -0.06 \pm 0.25$ given a top-quark mass of

175 GeV/c^2 and set an upper limit on f_{V+A} of 0.29 at the 95% confidence level; an improvement by a factor of 2 on the previous best direct limit.

1.1. Introduction. The decay of the top quark, the most massive fundamental particle observed for the first time by experiment [1, 2], is particularly interesting as a direct probe of the charged current weak interaction at the highest energy scale presently available. In the Standard Model, the spin-1/2 top quark decays via the charged current weak interaction to a spin-1 W^+ boson and a spin-1/2 b quark *, with a branching fraction above 99% and width $\Gamma_t = 1.4$ GeV [31] for a top-quark mass of 175 GeV/c^2. The lifetime of the top quark, $\hbar/\Gamma_t \sim 5 \cdot 10^{-25}$ s, is by an order of magnitude shorter than the typical strong interaction time scale for binding of quarks into hadrons, $\hbar/\Lambda_{\rm QCD} \sim 3 \cdot 10^{-24}$ s. Therefore, the top quark decays before hadronization, and the spin information is directly transferred to the decay products.

In the limit $m_b \to 0$, the pure charge current $V - A$ theory of the weak interaction (with coupling $-i\dfrac{g}{\sqrt{2}}V_{tb}\,\gamma^\mu(1-\gamma_5)$) predicts that the b quark has left-handed ($-1/2$) polarization (helicity), and the W^+ boson can only have either longitudinal (zero) or left-handed (-1) polarization. The right-handed ($+1$) polarization is forbidden. The fraction f_0 of W^+ bosons with longitudinal polarization is predicted to be $f_0 \approx 0.70$ [9] at leading order in perturbation theory. The nonzero b-quark mass and the higher-order QCD and electroweak radiative corrections modify these predictions below the 1% level [10, 32, 33]. However, the presence of nonstandard-model couplings in the Wtb vertex could significantly modify the polarization of the top-quark decay products [9, 34, 36]. Previous results have either been limited by the small statistics of the top-quark samples [11, 37–38] or have only set indirect limits [39, 40].

In this analysis (by CDF), the structure of the weak interaction is investigated by measuring the helicity fractions of the W boson in the top-quark decays. In order to discuss which couplings in the Wtb vertex could have an impact on the W-helicity fractions, the interaction Lagrangian for the most general coupling is considered below. The interaction of fermions and gauge bosons in general, can be expressed by six form factors, f, with a particular energy scale at which new physics may be opened. Assuming the W boson to be *on-shell*, the form factors can be reduced even to four.

While weak interactions have been tested with high precision at low-momentum transfers, e.g., in radioactive β decay, the vertex structure may be altered in interactions at high momentum transfers due to possible new physics contributions. Among the known fundamental particles, the top quark stands out

*Charge conjugate decays, with replacement of left-handed by right-handed polarization, are implicit. Results [68] contain analysis of 2.7 fb^{-1} (2010), see on p. 14.

as the heaviest, with a mass of $m_t = (173.3 \pm 1.1(\pm 0.6 \pm 0.9))$ GeV/c^2 [6], and thereby gives access to high momentum scales. It has been suggested that the top quark may have nonuniversal gauge couplings as a result of dynamical breaking of the electroweak symmetry [7]. Given our present knowledge of the Cabibbo–Kobayashi–Maskawa quark-mixing matrix [8], the top quark decays with a branching ratio (as we told above) close to 100% in the mode $t \to bW^+$. The Dirac structure of the Wtb vertex can be generalized by the interaction Lagrangian

$$L = \frac{g_\omega}{\sqrt{2}}\left[W_\mu^- \bar{b}\gamma^\mu (f_1^L P_- + f_1^R P_+)\, t - \right. \\ \left. - \frac{1}{m_W}\partial_\nu W_\mu^- \bar{b}\sigma^{\mu\nu}(f_2^L P_- + f_2^R P_+)t\right] + \text{h. c.}, \quad (1)$$

where $P\pm = 1(1 \pm \gamma^5)$ and $i\sigma^{\mu\nu} = -(1/2)|\gamma^\mu, \gamma^\nu|$ [9].

Four form factors $f_{1,2}^{R,L}$ can assume complex values in general, but take values of $f_1^L = 1$ and $f_1^R = f_2^L = f_2^R = 0$ in the standard electroweak theory in approximation of zero b-quark mass, such that the production of right-handed W bosons from top-quark decay is suppressed.

It is supposed that the production of longitudinally polarized W bosons is enhanced due to the large Yukawa coupling of the top quark to the Higgs field responsible for electroweak symmetry breaking (EWSB). The fraction of right-handed W bosons, f_+, is predicted by SM to be very small $\approx O(10^{-4})$ [10], which is well below the sensitivity of the measurements reported here. The partial decay widths into the different W-boson helicity states explicitly depend on the form factors. Assuming the standard electroweak theory values for the form factors, the fraction of longitudinally polarized W bosons is given by $f_0 = \Gamma(W_0)/[\Gamma(W_0)+\Gamma(W_-)+\Gamma(W^+)] \approx m_t^2/(2m_W^2+m_t^2) \approx 0.7$ [9], more precise the theory predicts $f_0 = 0.697 \pm 0.002$ at leading order in perturbation theory, where W_0 and $W_\pm$ indicate longitudinally and transversely polarized W bosons, respectively; for m_t as given above and a W-boson mass of $m_W = (80.403 \pm 0.029)$ GeV/c^2 [8]. Next-to-leading-order corrections decrease the total decay width, as well as $\Gamma(W_0)$, by about 10% [12], while f_0 is only changed by about 1% [10]. A significant deviation of f_0 or f_+ from the predictions exceeding the 1% level would be a clear indication of new physics.

This article reports the results of two analyses using the same dataset and their combination. Both analyses use the observable $\cos\theta^*$, which is the cosine of the decay angle between momentum of the charged lepton in the W-boson rest system and direction of the top-quark momentum that corresponds to the line between the production point and the decay point of W boson. This has the

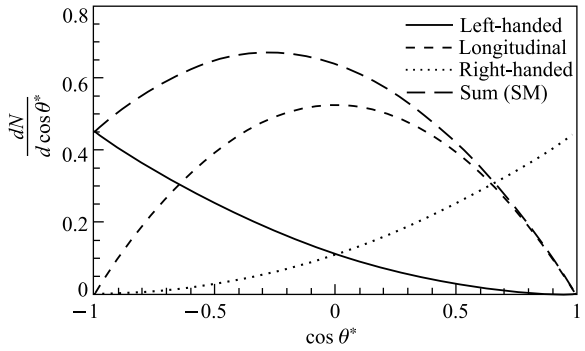

Fig. 1. Theoretically calculated $\cos\theta^*$ distributions for left-handed, longitudinally and right-handed polarized W bosons. The solid black line indicates the $\cos\theta^*$ distribution as expected in the Standard Model

following distribution:

$$\omega(\theta^*) = f_0\omega_0(\theta^*) + f_+\omega_+(\theta^*) + (1 - f_0 - f_+)\omega_-(\theta^*) \tag{2}$$

with

$$\begin{gathered}\omega_0(\theta^*) = \frac{3}{4}(1 - \cos^2\theta^*), \quad \omega_+(\theta^*) = \frac{3}{8}(1 + \cos\theta^*)^2, \\ \omega_-(\theta^*) = \frac{3}{8}(1 - \cos\theta^*)^2, \quad \omega(\theta^*) = \frac{dN}{d\cos\theta^*}.\end{gathered} \tag{3}$$

The parameters f_0 and f_+ are the W-boson helicity fractions to be determined. The two analyses estimate $\cos\theta^*$ for each event by reconstructing the full $t\bar{t}$ kinematics. These methods of reconstructing the four-vectors of the top quark and antitop quark as well as their decay products [13–15] possess a broad applicability and offer the possibility to measure a full set of top-quark properties, such as the top-quark mass and the forward–backward charge asymmetry in $t\bar{t}$ production [16]. Experimental acceptances and resolutions introduce distortions of the $\cos\theta^*$ distribution which must also be taken into account. The two analyses employ alternative methods for reconstructing the $t\bar{t}$ kinematics, for correcting the experimental effects, and for determining the polarization fractions from the resulting $\cos\theta^*$ distributions in the observed events (Fig. 1). They have similar sensitivities and are combined, taking into account correlations, to yield the most precise estimates of f_0 and f_+.

Both analyses subject the observed data to fits in three different scenarios:

1. Measure f_0 under the assumption that $f_+ = 0$. This corresponds to a model in which the form factors f_1^R and f_2^L are zero, meaning there are no right-handed bottom-quark couplings present.

2. Measure f_+ under the assumption that $f_0 = 0.7$, which is sensitive to models with $f_2^L = f_2^R = 0$, i.e., the presence of an additional $V + A$ current in top-quark decay, but no additional magnetic couplings. Using the relation $f_+/f_- = (f_1^R/f_1^L)^2$ one can translate the measured helicity fractions into the ratio of form factors.

3. Measure f_0 and f_+ simultaneously in a two-parameter fit, which is model-independent.

Model-dependent measurements of f_0 and f_+ using smaller datasets have been previously reported by the CDF [3], DØ [16, 17] Collaborations. Most recently the DØ Collaboration has reported a model-independent result using 1 fb^{-1} [17] of Tevatron data. The measurements reported here [4] use twice as much data compared to old data and improved analysis techniques and yield the most precise determinations of the W-helicity fractions in top-quark decays [8].

1.2. Selection of $t\bar{t}$ Candidate Events. The data used for the analyses reported here are collected by the CDF II detector. A detailed description of the Collider Detector at Fermilab (CDF) can be found elsewhere [29, 41]. A coordinate system with the z axis along the proton beam, azimuthal angle ϕ and polar angle θ are used. The pseudorapidity is defined as $\eta = -\ln(\tan(\theta/2))$. The transverse energy of a particle is defined as $E_T = E\sin\theta$.

Authors select events of the type $t\bar{t} \to W^+bW^-\bar{b} \to \ell\nu q\bar{q}'b\bar{b}$ which yield an experimental signature of one high-energy charged lepton, missing transverse energy due to the undetected neutrino, and at least four jets, two of which are b-quark jets. Exactly one isolated electron candidate with transverse energy $E_t > 20$ GeV and pseudorapidity $|\eta| < 1.1$ is required, or exactly one isolated muon candidate with transverse momentum* $P_T > 20$ GeV/c and $|\eta| < 1.0$. An electron or muon candidate is considered isolated if the E_T not assigned to the lepton in a cone of $R = \sqrt{(\Delta\eta)^2 + (\Delta\phi)^2} = 0.4$ centered around the lepton, is less than 10% of the lepton E_T or P_t, respectively. Jets are reconstructed by summing calorimeter energy in a cone of radius $R = 0.4$. The energy of the jets is corrected for differences as a function of η, time, and additional energy depositions due to multiple interactions occurring in the same event [18]. An additional correction leads from calorimeter based jets to jets at the particle level. Candidate jets must have corrected $E_T > 20$ GeV and detector $|\eta| < 2$. The corrected missing transverse energy E_T accounts for the energy corrections made for all jets with corrected $E_T > 12$ GeV and $|\eta| < 2$. for muons and is required to be greater than 20 GeV. At least one jet in the event must contain a secondary vertex identified

*As it is told above, there is used a cylindrical coordinate system, where the z axis is along the proton beam direction and θ is the polar angle. Pseudorapidity is $\eta = -\ln(\tan(\theta/2))$, while transverse momentum is $p_T = |p|\sin\theta$ and transverse energy is $E_T = E\sin\theta$. Missing transverse energy, E_T, is defined as the magnitude of $E_T = -\Sigma_i E_T^i n_i$ where n_i is the unit vector in the azimuthal plane that points from the beam line to ith calorimeter tower. Also $E_T = |E_T|$.

using the algorithm described in [19] with $|\eta| < 1.1$ and consistent with having originated from a b-hadron decay. Additional requirements further reduce the background contribution as follows. Electron events are rejected if the electrons originate from a conversion of a photon. Cosmic ray muon events are rejected as well. To remove Z bosons, events in which the charged lepton can be paired with any more loosely defined jet or lepton to form an invariant mass consistent with the Z peak, 76–106 GeV/c^2, are excluded.

With these selection criteria, we select 484 $t\bar{t}$ candidates in a sample corresponding to a total integrated luminosity of 1.9 fb^{-1}.

Kinematics resolutions and selection and reconstruction efficiencies for $t\bar{t}$ events are determined utilizing PYTHIA [20] and HERWIG [21] event generators where the top-quark mass is set to 175 GeV/c^2. Samples of events generated with PYTHIA, ALPGEN [22], and MADEVENT [23], interfaced to PYTHIA parton showering are used to determine certain background rates and to estimate the $\cos\theta^*$ distribution for background events. In order to develop and validate the methods presented, MADEVENT and a custom version of HERWIG are used to generate samples of simulated events with controllable W-boson helicity fractions. All generated events are passed through the CDF detector simulation [24] and then reconstructed in the same way as the observed events.

Table 1. **Expected number of background events and the number of all observed events in a 1.9 fb^{-1} data sample using the selection criteria described in the text**

Background source	N ($\geqslant 4$ jet)
W + heavy flavor	37 ± 10
Mistags	20 ± 5
Non-W	18 ± 16
Electroweak	12 ± 1
Total background	87 ± 23
Observed events	484

1.3. Background Estimation. The selected $t\bar{t}$ sample is estimated to be contaminated with about 87 events coming from background processes. These non-$t\bar{t}$ processes originate mainly from W + jets events with a falsely reconstructed secondary vertex (Mistags), fromt W + jets events in which the jets are real b- and c-quark jets (W + heavy flavor), and multijet processes that contain no real W boson (non-W). These backgrounds are estimated using a combination of data and Monte Carlo methods as described in detail in [19]. Additional sources of background arise from electroweak processes like diboson production (WW, WZ, ZZ), the production of single top-quarks, and Z bosons. These backgrounds are predicted based on their theoretical cross sections and acceptances and efficiencies, which are derived from simulated events. Table 1 shows the background estimation and the observed number of events after all selection criteria.

1.4. Boson Helicity Fractions. In order to measure the W-boson helicity fractions there were used two approaches. Both analyses use $\cos\theta*$ as the sensitive observable, estimated on an event-by-event basis by fully reconstructing the $t\bar{t}$ kinematics. The $\cos\theta*$ distribution can be decomposed into three separate

components according to the three different W-boson helicity states. The first analysis is based on the methods developed to precisely measure the top-quark mass [13] and uses the fact that the three helicity components have distinguishable shapes. In this technique were found the expected distributions («templates») of the helicity components, containing resolution effects, and superposed those. The helicity fractions are then given by normalizations from an unbinned likelihood fit and the results are corrected for acceptance effects afterwards [25]. Authors refer to this analysis as the «template» analysis in the following.

The second analysis, called the «convolution analysis», is based on the method described in [3, 14, 15]. Starting from the theoretically predicted number of events in each bin of the particle level $\cos\theta^*$ distribution, authors convolute acceptance and resolution effects with these predictions to derive the expected number of events in each bin of the reconstructed $\cos\theta^*$ distribution. In this method, f_0 and f_+ are then determined from a binned likelihood fit.

The event selection and reconstruction of the two techniques employ different choices in the design of background suppression, jet flavor identification, and parton assignment. The agreement between the two methods shows that these design choices *do not bias the final result.* While the convolution analysis uses the standard event selection described in Subsec. 1.2, the template analysis chooses to place an additional cut on the scalar sum of all transverse energies of the event, H_t, and requires $H_t > 250$ GeV to further suppress multijet non-W background. This results in (53 ± 20) events estimated as background, and reduces the total number of selected events to 430. A combinatoric ambiguity arises in the reconstruction of the $t\bar{t}$ kinematics when choosing which of the reconstructed jets corresponds to which of the final state quarks in the $t\bar{t} \to \ell\nu q\bar{q}' b\bar{b}$ decay. We analyse all possible jet-quark assignments and then use alternative criteria to choose the «best» one for each event. The template analysis uses the technique described in [13]: jet energies float within expected resolutions, b-tagged jets are assigned to b quarks, and the top-quark mass is left floating in the fit while the W-boson masses are constrained to 80.4 GeV/c^2.

The algorithm described in [3, 14, 15] is used in the convolution analysis. The jet-quark assignment is selected using constraints on the W-boson mass, the $t\bar{t}$ pairs mass difference, the transverse energy in the reconstructed $t\bar{t}$ pair with respect to the total transverse energy in the event, and the b-jet probability of the jets. Neither analysis assumes a particular value for m_t in the reconstruction; since f_0 has an explicit m_t-dependence, because doing so would introduce a bias in the measurement. Although the algorithms to reconstruct the kinematics of the $t\bar{t}$ pairs are different, the $\cos\theta^*$ resolution for each analysis is estimated to be the same (≈ 0.35 events).

In both analyses, the W-boson helicity fractions are determined from maximum likelihood fits to the resulting $\cos\theta^*$ distributions. The two analyses employ alternative methods to derive the fit inputs which will be discussed in more

detail in the next paragraphs. In the fits, the helicity fractions f_0 and f_+ are free parameters, the constraint $f_- = (1 - f_0 - f_+)$ is applied, and the background contribution is allowed to float but is Gaussian-constrained using an RMS corresponding to the uncertainty on the estimate of the total number of background events. As is already discussed, each analysis performs three different measurements (see introduction).

The template method utilizes samples of generated $t\bar{t}$ events in which the leptonically decaying W boson is forced to a specific polarization to get the normalized $\cos\theta^*$ probability distribution function $P(\cos\theta^*)$ for each W-boson polarization. These generated events satisfy all the selection criteria and are reconstructed in the same manner as the observed events. The $P(\cos\theta^*)$ for a certain helicity mode is obtained by fitting the reconstructed $\cos\theta^*$ distribution obtained from the corresponding generated $t\bar{t}$ events and does not depend on the helicity fractions assumed for the hadronically decaying W boson. The background modeling is verified by comparing the distribution obtained from generated events to the distribution of observed events in which there is no secondary vertex tag and in those for which the decay length of the secondary vertex tag is negative, meaning that the reconstructed secondary vertex and the reconstructed jet itself are located in opposite hemispheres with respect to the primary vertex. These are background dominated samples.

The $P(\cos\theta^*)$ parameterizations are empirically chosen to provide $\cos\theta$* use two exponential functions. The resulting $P(\cos\theta^*)$ are compared in Fig. 2. Using alternative fit functions negligibly affects the results.

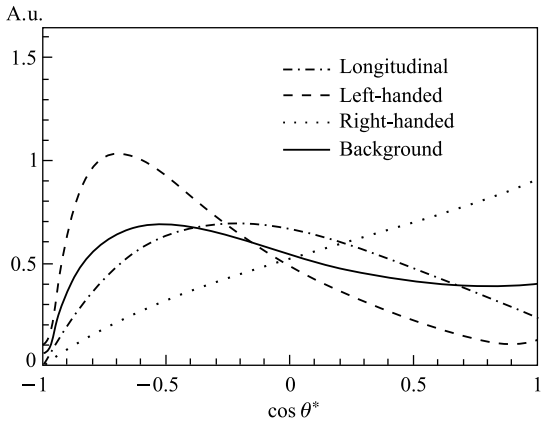

Fig. 2. $P(\cos\theta$*$)$ used in the template analysis, which are the reconstructed $\omega(\theta$*$)$ distributions for longitudinal, right- and left-handed W-boson helicities, as well as the $\omega(\theta$*$)$ in the background model. The curves are normalized to the same area

Since the kinematics of the W-boson decay depends on its polarization, the kinematic cuts applied have different acceptances for the different polarizations. Therefore a correction is applied to the obtained helicity fractions to account for these acceptance effects before presenting the results.

In the convolution analysis the $\cos\theta^*$ distribution is reconstructed in six bins, corresponding to the resolution of the reconstruction of the $t\bar{t}$ kinematics. The starting point for the extraction of the W-boson helicity fractions in this method is the theoretically predicted number of signal events in each bin of the $\cos\theta^*$ distribution, $\mu^{\mathrm{sig}}(f_0, f_+)$, depending on f_0 and f_+, which can be calculated using Eq. (2).

Acceptance and resolution effects are then taken into account [3] by convoluting both effects with theory prediction. This leads to the number of signal events expected to be observed in a certain bin accounting for all distorting effects:

$$\mu_k^{\mathrm{sig,obs}}(f_0, f_+) \propto \Sigma \mu_i^{\mathrm{sig}}(f_0, f_+)\varepsilon_i S(i,k). \tag{4}$$

The migration matrix element $S(i,k)$ gives the probability for an event which was generated in bin i to occur in bin k of the reconstructed $\cos\theta^*$ distribution. Since the acceptance depends on $\cos\theta^*$, the contribution of each bin was weighted with its event selection efficiency ε_i. The effects considered are independent of the W-boson helicity fractions and this is validated using several samples of generated events with different W-boson polarizations. Thus, ε_i and $S(i,k)$ can be estimated from a sample of events generated with the PYTHIA event generator. The total number of events expected to be observed in a certain bin is then given by the sum of $\mu_k^{\mathrm{sig,obs}}(f_0, f_+)$ and the expected number of background events, which is independent of the W-boson polarization and is derived from the background composition shown in Table 1.

In a maximum-likelihood fit the expected number of events is compared bin by bin to the number of observed events to determine f_0 and f_+.

In order to compare the observations with theory, there was subtracted the background estimate from the reconstructed $\cos\theta^*$ distribution, corrected for acceptance and resolution, and normalized the distribution to the $t\bar{t}$ cross section of $\sigma_{t\bar{t}} = (6.7 \pm 0.9)$ pb [24, 26]. The correction is made by applying a bin-by-bin correction factor to the $\cos\theta^*$ distribution. The correction factor is given by $\mu_i^{\mathrm{sig}}\ (f_0^{\mathrm{fit}}, f_+^{\mathrm{fit}})$ divided by $\mu_k^{\mathrm{sig,obs}}(f_0^{\mathrm{fit}}, f_+^{\mathrm{fit}})$, where f_0^{fit} and f_+^{fit} are the obtained results.

The systematic uncertainties associated with the measurement of f_0 and f_+ are summarized in Table 2. The systematic uncertainties were determined by constructing ensemble tests with signal and/or background templates, affected by the systematics under study, but fit using the default parameterizations and normalizations described above. The authors studied the influence of variations in the jet energy scale (JES) and of variations in initial and final state radiation

Table 2. **The sources of systematic uncertainties and their related estimates for the template analysis (templ.) and the convolution analysis (conv.). The total systematic uncertainty is taken as the quadrature sum of the individual sources**

Source	δf_0 (f_+ fixed)		δf_+ (f_0 fixed)		δf_0 (combined fit)		δf_+ (combined fit)	
	templ.	conv.	templ.	conv.	templ.	conv.	templ.	conv.
JES	0.024	0.045	0.017	0.025	0.021	0.016	0.027	0.032
ISR	0.002	0.010	0.003	0.003	0.010	0.036	0.007	0.014
FSR	0.021	0.025	0.009	0.011	0.025	0.045	0.002	0.016
Bkg	0.023	0.032	0.016	0.019	0.018	0.028	0.017	0.032
MC	0.019	0.012	0.009	0.005	0.019	0.015	0.010	0.002
PDF	0.005	0.005	0.005	0.002	0.005	0.014	0.002	0.006
Total	0.044	0.062	0.027	0.034	0.043	0.072	0.034	0.050

(ISR, FSR). The latter was estimated by producing samples of simulated events for which the simulation was altered to produce either less or more gluon radiation compared to the standard setting [13]. Specifically, two parameters controlling the parton shower in the PYTHIA program are varied: Λ_{QCD} and the scale factor K to the transverse momentum scale of the showering. The different settings are derived from studies of ISR in Drell–Yan events. The authors also studied the influence of the background modeling (Bkg), of different Monte Carlo event generators (MC), and of the parton distribution function (PDF). The resulting shifts in the mean fitted longitudinal and right-handed fraction are used to quantify the systematic uncertainties.

The positive and negative variations obtained are symmetrized by choosing the maximum deviation. The ensemble tests were all performed using PYTHIA generated events with $m_t = 175$ GeV/c^2 as a signal with the W-boson helicity fractions $f_0 = 0.70$ and $f_+ = 0.0$, and the background model as described above. It was verified that these uncertainties do not depend on the actual value of f_0 and f_+ by fitting samples of generated events with different W-boson polarizations.

The analyses presented in this paper use a top-quark mass of 175 GeV/c^2. Since f_0 explicitly depends on the top-quark mass, the dependency of the measured value of f_0 on the top quark mass is not treated as a systematic uncertainty. The measured value of f_+ is only negligibly affected by variations in the assumed top-quark mass.

1.5. Results for f_0 and f_+ and Combination of the Results. The $\cos\theta^*$ distribution from the observed events is shown in Figs. 3 and 4 for both analyses together with the fits for f_0 and f_+ and the model independent measurement.

The results for the three different measurements together with the statistical and systematical uncertainties in both analyses are summarized in Table 3. In the

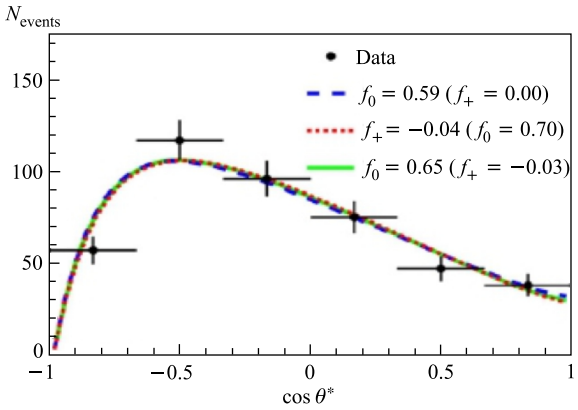

Fig. 3. The observed $\cos\theta^*$ distribution (points) overlaid with the fit — curves for the three different fit scenarios (as explained in Subsec. 1.1) for template analysis. All curves coincide

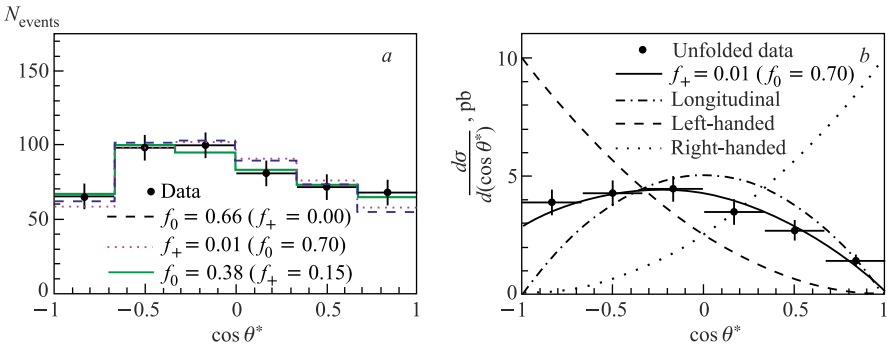

Fig. 4. *a*) The observed $\cos\theta^*$ distribution (points) is presented overlaid with the fits for f_0 and f_+ for the convolution analysis. *b*) The deconvoluted (using the fit result of the f_+ measurement) distribution normalized to the $t\bar{t}$ cross section is shown together with the theoretically predicted curves for purely left-handed, right-handed, and longitudinally polarized W bosons

template analysis the correlation between f_0 and f_+ is determined to be -0.87 in the simultaneous fit, while for the convolution analysis the correlation is -0.89.

There were combined the single results accounting for correlations using the BLUE method [27]. The combined results can be found in Table 3. The statistical correlation between both analyses is estimated from ensemble tests using samples of generated events which account for the event overlap in the signal contribution. For the two model-dependent scenarios the correlation coefficients are found to be 0.66 and 0.65 when fitting for f_0 or f_+, respectively. The correlation matrix for the model-independent scenario is given in Table 4. The resulting combination

Table 3. **Results of the template analysis, the convolution analysis, and the combined values. The results are given together with their statistical and systematical uncertainties. In addition the χ^2/dof of the combination is given**

Fractions	Template	Convolution	Combination	χ^2/dof
$f_0(f_+ = 0.0)$	$0.59 \pm 0.11 \pm 0.04$	$0.66 \pm 0.10 \pm 0.06$	$0.62 \pm 0.10 \pm 0.05$	0.7/1
$f_+(f_0 = 0.0)$	$-0.04 \pm 0.04 \pm 0.03$	$0.01 \pm 0.05 \pm 0.03$	$-0.04 \pm 0.04 \pm 0.03$	1.8/1
f_0	$0.65 \pm 0.19 \pm 0.04$	$0.38 \pm 0.21 \pm 0.07$	$0.66 \pm 0.16 \pm 0.05$	4.3/2
f_+	$-0.03 \pm 0.07 \pm 0.03$	$0.15 \pm 0.10 \pm 0.05$	$-0.03 \pm 0.06 \pm 0.03$	4.3/2

Table 4. **Correlation matrix for combining the template and convolution analyses in the model-independent scenario**

Fractions	Template f_0	Convolution f_0	Template f_+	Convolution f_+
Template f_0	1.00	0.45	-0.87	-0.40
Convolution f_0	0.45	1.00	-0.42	-0.89
Template f_+	-0.87	-0.42	1.00	0.48
Convolution f_+	-0.40	-0.89	0.48	1.00

is weighted towards the template determination of f_+ since its total uncertainty is significantly smaller than the total uncertainty from the convolution method. Due to the strong anticorrelation between f_0 and f_+ (see Table 4) the f_0 determination is affected correspondingly.

The systematic uncertainties are taken to be completely correlated between the two methods. When combining the model-independent results, the systematic uncertainties for f_0 and f_+ are taken to be 100% anticorrelated. The combined values of f_0 and f_+ have a correlation of -0.82. The combination improves the sensitivity by about 10% relative to the measurements of either method separately.

In conclusion, the authors present two different analyses and their combination determining the W-boson helicity fractions in top-quark decays, giving the world's most sensitive result for measuring these fractions so far. In addition, to measure f_0 and f_+ separately, while fixing the other parameter to its expected value, there was present a model-independent simultaneous measurement of the two fractions. All of these results are consistent with the values predicted within the electroweak theory of the Wtb vertex.

For the suitable demonstration of the common CDF preliminary results on the W fractions we present Fig. 5. Here are simultaneously shown template and convolution (unfolding) on the W-helicity fractions at the same luminosity 1.9 fb^{-1} the same as in Table 3. Besides, here is presented the matrix element method that was not discussed in the main text (reported in Conference [27, 28] preliminary, [47]).

1.6. Search for $V + A$ Current in Top-Quark Decays in $p\bar{p}$ Collisions at $\sqrt{s} = 1.96$ TeV. As was shown, the fraction of W boson in the Standard Model from the top-quark decay f_1^L is equal to one, while the three other form factors

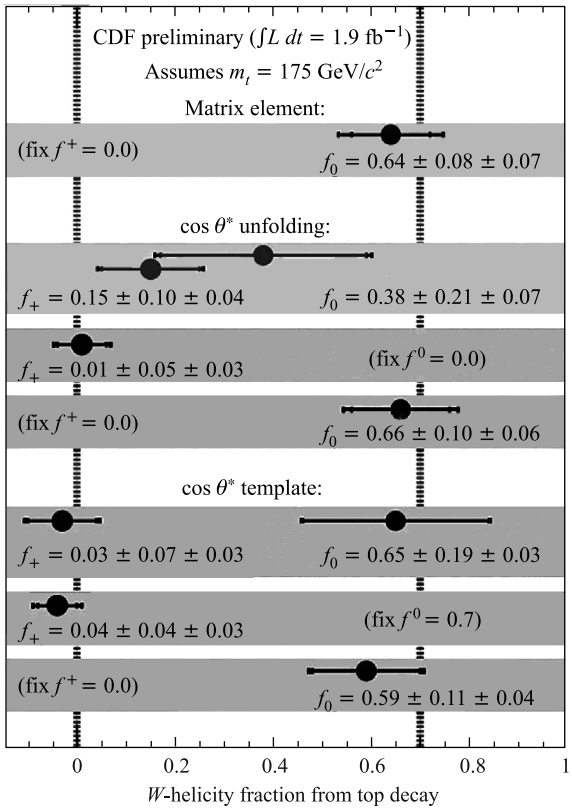

Fig. 5. Comparison of the W-helicity fraction results that were received by different methods at the same integral luminosity. Starting from «$\cos\theta^*$ unfolding» (convolution) these data are the same as in Table 3. In addition are shown recent results of [68] (2010) with model-independent $f_0 = 0.88 \pm 011(\text{stat.}) \pm 0.06(\text{syst.})$, $f_+ = -0.15 \pm 0.07(\text{stat.}) \pm 0.06(\text{syst.})$, and with constraining $f_+[f_0]$ to 0.0 and [0.70} yields: $f_0 = 0.70 \pm 0.07(\text{stat.}) \pm 0.04(\text{syst.})$, $f_+ = -0.01 \pm 0.02(\text{stat.}) \pm 0.05(\text{syst.})$

$(f_1^R, f_2^{R,L})$ are all equal to zero, leading to a pure $V - A$ structure of the weak interaction. This $V - A$ structure predicts that the W bosons from the top-quark decays are dominantly either longitudinally polarized or left-handed, while right-handed W-boson decays are heavily suppressed or even forbidden in the limit of a massless b quark. Assuming a top-quark mass of 175 GeV/c^2, the fraction of longitudinally polarized W bosons is predicted to be $f_0 = 0.7$, while the fraction of left-handed W bosons is $f_- = 0.3$. A significant deviation from the predicted value for f_0 or a nonzero value for the right-handed fraction f_+ could indicate new physics, such as a possible $V + A$ component in the weak interaction or other

anomalous couplings at the Wtb vertex. (The W-boson polarization manifests itself in the decay $W \to \ell\nu_\ell$ at the angle θ^*, see Fig. 1.)

In this letter [30], the authors made an attempt to search for a $V + A$ current in the top-quark decay, while assuming that the $t\bar{t}$ production mechanism is in agreement with the standard model prediction. Further it is assumed the absence of couplings from magnetic moment interactions in the Wtb interaction, so that f_0 is unchanged from 0.70 [9]. Then, the $V + A$ fraction f_{V+A} is related to the fraction f_+ of right-handed W^+ bosons by $f_{V+A} = f_+/(1 - f_0)$, and the $V - A$ fraction $f_{V-A} \equiv 1 - f_{V+A}$ is related to the fraction f_- of left-handed W^+ bosons by $f_{V-A} = f_-(1 - f_0)$. The W^+-boson polarization can be inferred (as earlier) from the angular distribution of the charged lepton (e or μ) in the decay $W^+ \to \ell^+ v$.

The authors have introduced the observable $M^2_{\ell b}$ — the square of the invariant mass of the charged lepton and the jet from the b quark, which is related to $\cos\theta^*$ by $M^2_{\ell b} \cong (1/2)(m_t^2 - m_W^2)(1 + \cos\theta^*)$.

The relation is exact in the limit $m_b \to 0$.

This search is based on a data set with an integrated luminosity of approximately 700 pb^{-1} acquired by the Collider Detector at Fermilab (CDF II) [11, 29].

There were studied three independent data samples enriched in $t\bar{t}$ events. Two of the data samples are in the lepton $+$jets channel, with $t\bar{t} \to W^+bW^-b$ events where one of the W bosons decays hadronically and the other leptonically. The lepton $+$jets event selection requires one isolated lepton with $E_T > 20$ GeV, $\not\!\!E_T > 20$ GeV, at least three jets with $E_T > 15$ GeV, and one or two b-tagged jets. More details on the selection, the b-tagging procedure, and the sample composition can be found in [40]. The authors model the hard $t\bar{t}$ process with the Monte Carlo (MC) event generator ALPGEN [22] with CTEQ5L [42] parton densities and PYTHIA [20], under the assumption that the top-quark mass is 175 GeV/c^2, and simulate the detector response using GEANT [43, 44]. For $t\bar{t}$ production with $V - A$ top-quark decay, there was estimated a selection efficiency, including the branching fraction, of $A_{V-A} = 3.4\%$ (1.2%) for events with one (two) b-tagged jets. Because of the lower average p_T of the charged lepton for $V - A$, this is a factor 0.92 below the efficiency for $V + A$.

For the lepton $+$ jets sample with single b-tagged jets (the b-tagged jet is from the same top-quark decay as the charged lepton) the number of the $t\bar{t}$ events is approximately half of the total $t\bar{t}$ events. The background $M^2_{\ell b}$ distribution is a combination of 85% from $W +$ jets, modeled by ALPGEN $Wb\bar{b}^-$, and 15% multijet events, modeled by nonisolated lepton $+$ jets data events. With the used model of the background in 695 pb^{-1}, it was observed 304 candidates with a total expected background of (88 ± 11) events.

For the lepton $+$ jets sample with two b-tagged jets (the two possible $M^2_{\ell b}$ values of the charged lepton) two possible combinations are used. In this way, the authors keep both the correct and incorrect combinations, and account for their

correlation. The background is modeled by ALPGEN $Wb\bar{b}$; here the multijet background is negligible. Nonuniform binning was applied in the 2-D $M^2_{\ell b}$ distributions in order to ensure sufficient MC events in each bin. In 695 pb^{-1}, the authors find 75 candidates with a total expected background of (9 ± 2) events.

The third sample is in the dilepton channel, with $t\bar{t} \to W^+bW^-\bar{b}$ events, where both W bosons decay leptonically. The dilepton event selection requires two identified leptons with opposite electric charge and $E_T > 20$ GeV, $\not\!\!E_T > 25$ GeV, and at least two jets with $E_T > 15$ GeV. More details on the selection and the sample composition can be found in [45]. For $t\bar{t}$ production with $V - A$ top-quark decay, modeled by ALPGEN as described above, there was estimated a selection efficiency, including the branching fraction, of $\varepsilon_{V-A} = 72\%$, a factor 0.88 below the efficiency for $V + A$.

The two possible $M^2_{\ell b}$ values for a charged lepton with either the highest or the second highest E_T jet, assumed to be produced by the fragmentation of the b quarks, are used to constract a 2-D distribution. As one can reconstruct $M^2_{\ell b}$ from the top-quark decay and from the antitop-quark decay, one makes one entry for each charged lepton. The effect of the correlation between the spins of the top-quark and the antitop-quark is negligible here. Again, nonuniform binning in the 2-D $M^2_{\ell b}$ distributions is applied.

The background $M^2_{\ell b}$ distribution is the combination of three background types: approximately 50% from $Z/\gamma^* \to \ell^+\ell^-$ with associated jets, 30% from $W \to \ell\nu$ with associated jets where a jet is misidentified as a lepton, and 20% from massive diboson pairs, WW/WZ. The Z/γ^* and diboson background $M^2_{\ell b}$ distributions are modeled by ALPGEN. The misidentified lepton background is based on inclusive lepton trigger data, where the second lepton is instead a jet (charged particle track) weighted by a probability for misidentification as an electron (muon). A background-dominated data sample with only one jet is consistent, in terms of both the rate and the shape of the $M^2_{\ell b}$ distribution, with the chosen model of the background. In 750 pb^{-1}, the authors observed 64 candidates ($12\,ee$, $24\,\mu\mu$, $28\,e\mu$) with a total estimated background of (20 ± 4) events.

The fraction f_{V+A} is estimated by comparing the $M^2_{\ell b}$ distribution in data with parent $M^2_{\ell b}$ distributions for $t\bar{t}$ production with $V - A$ top-quark decay ($f_{V+A} = 0.0$), $t\bar{t}$ production with $V + A$ top-quark decay ($f_{V+A} = 1.0$), and backgrounds. A binned log likelihood fit procedure is used to extract the parameter of interest, f_{V+A}. The authors represent the imperfectly known accepted background cross section for each sample, $\sigma_{\rm bg}$, and the $t\bar{t}$ cross section, [24, 26], $\sigma_{t\bar{t}}$, by nuisance parameters. The analytic expression for the likelihood for each sample,

$$L = \left[\prod_{i=0}^{N} P(n_i, \mu_i)\right] G(\sigma_{\rm bg}, \delta_{\sigma_{\rm bg}})\, G(\sigma_{t\bar{t}}, \delta_{\sigma_{t\bar{t}}}), \tag{5}$$

Table 5. **The input values for the nuisance parameters and the values from the best fit to the combined samples**

Nuisance parameter	Input, pb	Fit, pb
$\sigma_{t\bar{t}}$	6.7 ± 1.0	7.3 ± 0.9
$\sigma_{\rm bg}$ lepton + jets 1 b-tag	0.156 ± 0.017	0.154 ± 0.016
$\sigma_{\rm bg}$ lepton + jets 2 b-tag	0.013 ± 0.002	$0.013 \pm 0.0020.022$
$\sigma_{\rm bg}$ dilepton	0.026 ± 0.006	0.022 ± 0.006

is the product over all N bins in $M^2_{\ell b}$ of the Poisson probabilities of observing n_i entries in a given bin i, where the average expected bin content is μ_i and the Gaussian constraints on the estimated background and the predicted $t\bar{t}$ production cross sections, as shown in Table 5. The μ_i are given by:

$$\mu_i = N^{\rm data}[x_{V+A}T^i_{V+A} + x_{V-A}T^i_{V-A} + x_{\rm bg}T^i_{\rm bg}], \tag{6}$$

$$\begin{aligned} x_{V+A} &= \frac{f_{V+A}\varepsilon_{V+A}\sigma_{t\bar{t}}}{\sigma_{\rm bg} + \sigma_{t\bar{t}}[\varepsilon_{V+A}f_{V+A} + \varepsilon_{V-A}(1-f_{V+A})]}, \\ x_{V-A} &= \frac{(1-f_{V+A})\varepsilon_{V-A}\sigma_{t\bar{t}}}{\sigma_{\rm bg} + \sigma_{t\bar{t}}[\varepsilon_{V+A}f_{V+A} + \varepsilon_{V-A}(1-f_{V+A})]}, \\ x_{\rm bg} &= \frac{\sigma_{\rm bg}}{\sigma_{\rm bg} + \sigma_{t\bar{t}}[\varepsilon_{V+A}f_{V+A} + \varepsilon_{V-A}(1-f_{V+A})]}. \end{aligned} \tag{7}$$

Here $N^{\rm data}$ is total number of observed events for the sample.

The x_{V+A}, x_{V-A}, and $x_{\rm bg}$ are the fractions of $t\bar{t}$ production with $V+A$ top-quark decay, $t\bar{t}$ production with $V-A$ top-quark decay, and background, respectively. The T^i_{V+A}, T^i_{V-A}, and $T^i_{\rm bg}$ are the probabilities for an event to occupy bin i of the corresponding $M^2_{\ell b}$ distribution. Note that $\Sigma_i T^i = 1.0$. The combined likelihood is the product of the likelihoods of the three samples, but with one common Gaussian constraint on the $t\bar{t}$ cross section.

The robustness of the fitting procedure has been tested with MC simulated experiments. For a given experiment and a particular sample, the number of observed data events is distributed in three categories ($t\bar{t}$ production with $V+A$ top-quark decay, $t\bar{t}$ production with $V-A$ top-quark decay, and background) according to their expected fractions from Eqs. (6), (7). For each category, the events are generated from the relevant $M^2_{\ell b}$ parent distribution. The hypotheses that $f_{V+A} = 0.0, 0.1, \ldots, 1.0$ are studied for 2000 experiments for all samples combined, as well as for the three samples separately. In all cases, the fit is unbiased and stable. The authors find an expected statistical uncertainty of parent distribution 0.22 on f_{V+A} for the combined case, 0.27 for all lepton+jets events, with 0.35 for one b-tagged jet and 0.41 for two b-tagged jets, and 0.46 for

dilepton events. In all cases, this includes a small component ($\leqslant 0.2$) due to the uncertainties on the background and $t\bar{t}$ cross sections.

The maximum likelihood fit to the lepton + jets sample yields a value of $f_{V+A} = 0.21 \pm 0.28$, with $f_{V+A} = 0.16 \pm 0.36$ for the subset of events with one b-tagged jet and $f_{V+A} = 0.28 \pm 0.44$ for the subset of events with two b-tagged jets. For the dilepton sample, we obtain $f_{V+A} = -0.64 \pm 0.37$. The probability to obtain a value smaller than the dilepton result is 10% for the hypothesis $f_{V+A} = 0$. The lepton + jets and dilepton results are compatible at about 1.8 standard deviations.

The estimates of the systematic uncertainties on the measured value for f_{V+A} are shown in Table 6. for all samples combined. The leading sources of sys-

Table 6. **The systematic uncertainties on the measurement of f_{V+A} for all samples combined**

Source	Uncertainty
Jet energy	0.10
Background modeling	0.04
MC statistics	0.04
Initial/final state QCD radiation	0.02
Multiple $p\bar{p}$ interactions	0.02
b-tag efficiency (E_T)	0.02
MC generator	0.01
Parton densities	0.01
Total	0.12

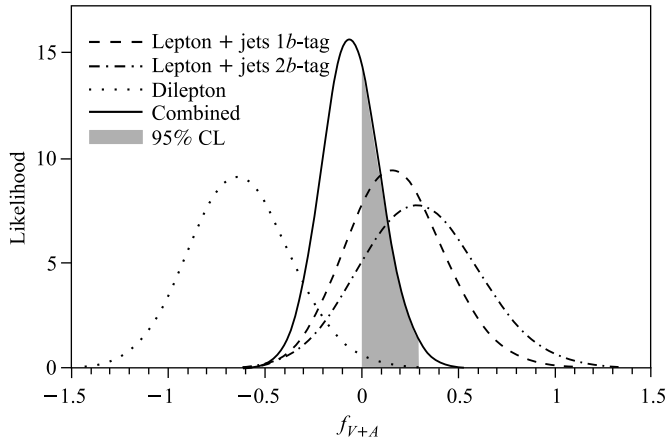

Fig. 6. Likelihood distribution (see Eq. (6)) for the lepton + jets and dilepton data samples separately and combined

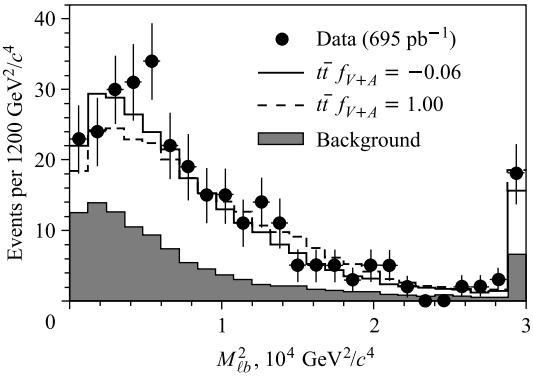

Fig. 7. The $M^2_{\ell b}$ distribution for the lepton + jets sample with one b-tagged jet. For $f_{V+A} = 0.06$, the χ^2 probability is 69%

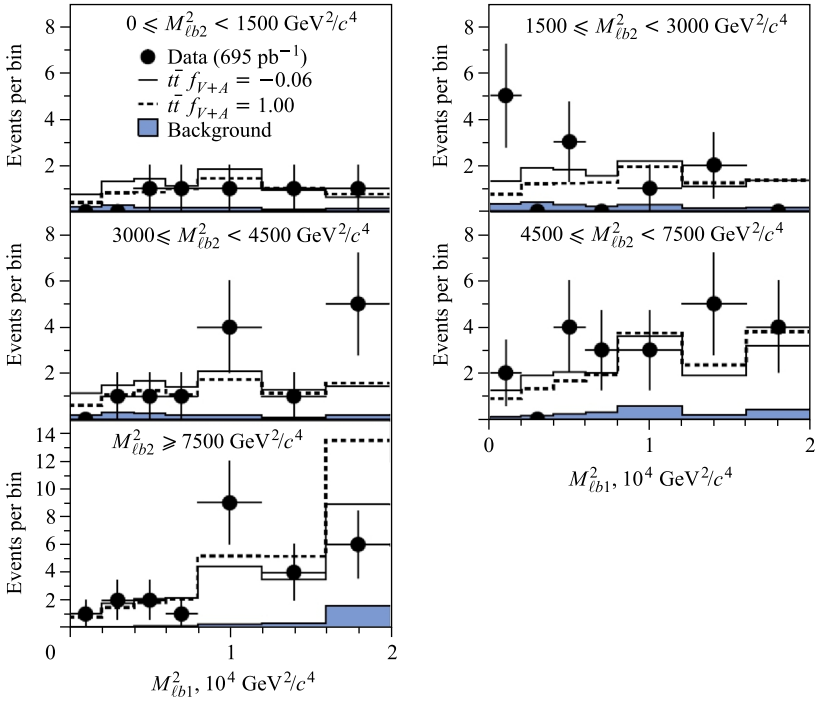

Fig. 8. $M^2_{\ell b1}$ distribution for the charged lepton and the highest E_T b-tagged jet, in five regions of $M^2_{\ell b2}$ for the charged lepton and the second highest E_T b-tagged jet, for the lepton + jets sample with two b-tagged jets. For $f_{V+A} = -0.06$, the χ^2 probabilities are 92, 3, 10, 18, and 47% in order of increasing $M^2_{\ell b2}$

tematic uncertainty arise from uncertainties on the measured jet energy [18], the background shape and normalization, and limited MC statistics.

All systematic uncertainties evaluated at $f_{V+A} = 0$; the authors find that the dominant uncertainty is insensitive to the value f_{V+A}. They quote result at top-quark mass value of 175 GeV/c^2, where the dependence of the measurement (upper limit) for f_{V+A} is $\pm 0.07(0.06)$ for a ± 2 GeV/c^2 shift in top-quark mass. Note, that many of the above sources of systematic uncertainty also contribute significantly to the systematic uncertainty on the measurement of the top-quark mass [8].

Combining samples, the result for the fraction of $V + A$ current in top-quark decay is

$$f_{V+A} = -0.06 \pm 0.22(\text{stat.}) \pm 0.12(\text{syst.}).$$

This value is in agreement with the Standard Model. Table 5 summarizes the fitted values for the nuisance parameters. The likelihood distribution is shown in Fig. 6 for the combined sample as well as for each individual sample. The good agreement in the $M^2_{\ell b}$ distribution between data and the best fit result for f_{V+A} from the combined sample is shown in Figs. 7–9, where the highest bins as well contain overflow entries. For comparison $f_{V+A} = 1.00$ is also shown.

Combining all samples, the authors set an upper limit on the fraction of $V+A$ current in the top-quark decay of $f_{V+A} < 0.29$ at 95% CL.

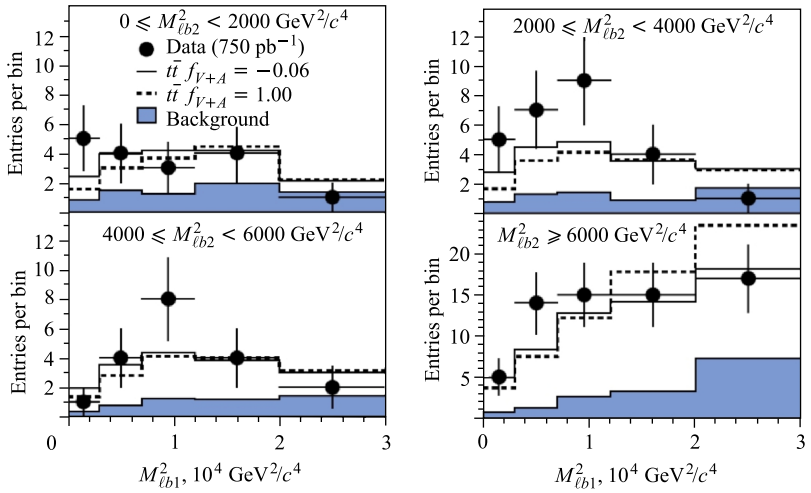

Fig. 9. $M^2_{\ell b1}$ distribution for a charged lepton and the highest E_T jet, in four regions of $M^2_{\ell b2}$ for a charged lepton and the second highest E_T jet, for the dilepton sample. There are two entries per event, one for each lepton. For $f_{V+A} = -0.06$, the χ^2 probabilities are 58, 14, 54, and 51% in order of icreasing $M^2_{\ell b2}$

This is an improvement by a factor of 2 on the previous best direct limit [11]. In terms of the fraction of right-handed W^+ bosons, the results are $f_+ = -0.02 \pm 0.07(\text{stat.}) \pm 0.04(\text{syst.})$ and $f_+ < 0.09$ at 95% CL.

Let us note that $f_+ < 0.26$ at 95% CL [3] is also consistent with SM predictions.

2. TOP-QUARK CHARGE DETERMINATION

2.1. Introduction. Under the Standard Model (SM) the top quark is an upper quark of the third generation with the electric charge of $+2/3$. Since its discovery in Tevatron experiments [1, 2], some of its properties have been measured and in all cases it appears that the top quark has the properties expected in the SM. On the other hand, in the analysis carried out by the CDF and DØ Collaborations, the correlations of the b quarks and W bosons in the process $p\bar{p} \to t\bar{t} \to W^+bW^-\bar{b}$ have not been determined (due to insufficient statistics). It means that at the time being the top quark electric charge is not measured and therefore one cannot exclude an alternative interpretation that is based on a conception of an exotic quark with charge $-4/3$, part of the fourth generation of quarks model [46], where the SM top quark also exists but its mass should be around 270 GeV. It should be stated that this conception is also not excluded by the present precision electroweak data, which are consistent with existence of an exotic quark of charge $-4/3$ and mass ≈ 170 GeV.

There are several techniques to determine the electric charge of the top quark at present collider experiments (Tevatron and LHC experiments are taken into account). Discussion on this subject can be found in [47] and [48]. Essentially there are two basic approaches based on:

- radiative $t\bar{t}\gamma$ processes,
- top-quark decay product charges.

In the case of the radiative $t\bar{t}\gamma$ processes, measurement of the top-quark electric charge (Q_{top}) is based on direct measurement of the top-quark electromagnetic coupling through photon radiation in $t\bar{t}$ events. Top quark can radiate a photon in the production as well as in the decay phase of the process. In the former case (radiative top production) the cross section is expected to be. In the latter case (radiative top decay: $pp(\bar{p}) \to t\bar{t}\gamma pp(\bar{p}) \to t\bar{t}\gamma, t \to Wb\gamma$) the situation is more complicated as the photon can be radiated also from the b-quark and W-boson line, and the cross section is not exclusively proportional to $\sigma_\gamma Q^2_{\text{top}}$, but nonetheless, depends on Q_{top}. To measure the top charge we need to distinguish between the radiative processes sensitive to Q_{top} and other radiative processes with the same experimental signature. This approach requires a high statistics to measure the rare radiative processes [48] therefore it is not applicable for the Tevatron experiments and can be investigated only at LHC [49].

The second approach of the top-charge measurement is based on the reconstruction of the charges of the top-quark decay products. The dominant decay channel of the top quark is that to the b quark via the charged current: $t \to W^+ b\,(\bar{t} \to W^- \bar{b})$. There are three main ingredients in the top-quark charge measurement: determination of the charge of the W boson using the decay lepton charge, $W^+ \to \ell^+ \nu_\ell\,(W^- \to \ell^- \bar{\nu}_\ell)$, pairing of the W and b jet to ensure that they are from the same top quark, and, at last, getting the flavor of the b jet, where a correlation between the charge of the b quark and the hadrons belonging to the b jet, which results from the hadronization process of the b quark, is used. This approach does not require high statistics and thereby is available also for the Tevatron experiments and we will describe the first results obtained in the frames of this approach.

The results on the top-quark charge study available at present come from the DØ experiment (based on 370 pb^{-1} of data) [50] and CDF experiment (base on an integrated luminosity of 1.5 fb^{-1}) [51]. We will rely mainly on the experiment CDF.

2.2. Data Selection. In the CDF experiment, the analysis was carried out on dilepton (DL) events ($t\bar{t} \to \ell^+ \nu \ell^- \bar{\nu} b \bar{b}$) and «lepton + jets» (LJ) ones ($t\bar{t} \to \ell^+ \nu j j b \bar{b}$). All $t\bar{t}$-jets events were not used due to a huge QCD background. Experimentally the data were collected with an inclusive lepton trigger requiring an electron or muon with $E_T > 18$ GeV. From the inclusive lepton dataset events were selected offline in accordance with selection criteria for the LJ and DL channel.

For LJ-type event the following selection criteria were used: a reconstructed isolated electron (muon) with E_T (in the muon case P_T) > 20 GeV, missing $E_T > 20$ GeV, and at least 3 jets with $E_T > 20$ GeV, and also the fourth jet with $E_T > 12$ GeV.

For dileptonic type of event the applied criteria were: at least two isolated, opposite-charged leptons, with $p_T > 20$ GeV, event missing transverse energy $E_T > 25$ GeV and away from any jet, at least 2 reconstructed jets with $p_T > 15$ GeV; and it was also required that the total transverse energy in the event $H_T = p_{T\,\mathrm{lep}} + p_{T\,\mathrm{jets}} + E_T$ be greater than 200 GeV.

To improve the signal-to-background ratio in both channels, it was required to have b jets identified by using the secondary vertex algorithm — b jet should contain a secondary vertex as a consequence of a B hadron having decayed. In the LJ (DL) channel at least two (one) b jets are required.

2.3. Pairing of W Bosons and b Jets. One of the key ingredients of the top-quark charge analysis is a correct pairing of W boson and b jet which ensures that both the W boson and the b jet come from the same branch of a top-quark decay. Identifying the W boson by means of its leptonic decay, it means that a correct pairing of the lepton and b jet is finally needed. In the LJ channel the lepton b-jet pairing is performed using the top-quark mass fitter with constraint

on top-quark and W-boson mass. Requiring two b-tagging, 4 combinations are possible for each candidate LJ event and the fitter provides for each of them χ^2. The combination with the lowest χ^2 is taken as the correct one. At the same time only the combinations with $\chi^2 < 9$ are taken. As a result, the obtained selection efficiency was 53% and the purity 86%. In the DL channel, the highest $2E_T$ jets were taken as the b jets and for the pairing of lepton and b jet the square of lepton and b-jet invariant mass $M^2_{\ell b}$ was used. From 4 possible values of $M^2_{\ell b}$ (2 for each ℓb combination) in each event as the right combination was taken the one which does not produce the largest value of $M^2_{\ell b}$. To increase the purity only events for which the maximum value of $M^2_{\ell b}$was greater than 21.000 GeV^2 were selected.

2.4. Jet-Charge Algorithm. In order to determine whether the b jet comes from a b quark or a $\bar{b}$ quark the following jet-charge algorithm was applied:

$$J_Q = \frac{\sum\limits_i Q\,(p_i j)^k}{\sum\limits_i (p_i j)^k}, \tag{8}$$

where $Q_i(p_i)$ is the charge (momentum) of the ith track, the j defines the b-jet axis direction and κ is a parameter which was optimized (for the best separation of b and $\bar{b}$ jets) to 0.5.

The jet charge algorithm being optimized on MC samples, was tested using a dijet data sample enriched in heavy flavor. Events were required to have a nonisolated muon with $p_T > 9$ GeV within a jet with $E_T > 20$ GeV (the so-called muon jet) and also another jet with $E_T > 20$ GeV which is back to back with the muon jet. Both these jets were required to be identified as b jets. Assuming that muon is from b-quark decay, its sign defines the flavor of the muon jet as well as the flavor of the away jet (it has an opposite flavor than the muon jet), and it enables us to define the jet charge purity as a fraction of events where the muon charge is opposite to the charge of away jet over the total number of selected events. Correcting the jet charge purity on effects like B mixing and charm decay, a scale factor between the purity obtained on data and that obtained on MC datasets was found to be $S_F = 1.01 \pm 0.01(\text{stat.}) \pm 0.02(\text{syst.})$.

2.5. Signal and Background Expectations. To distinguish between the SM and exotic model (XM) scenario we need to find the signal and background efficiencies purities expected for a given integrated luminosity (in our case 1.5 fb^{-1}). The combined efficiency is a product of the pairing efficiency and jet-charge efficiency. At the combined purity it should be taken not only the paring purity (p_{pair}) and jet charge purity (p_{J_Q}) but also a probability that the b jet would be misidentified ($f_{\text{non}\,b}$) and also the corresponding scale factors between data and MC for the p_{J_Q} and $f_{\text{non}\,b}$, i.e., $S_F^{J_Q}$ and $S_F^{\text{non}\,b}$, respectively. Finally, for the combined

purity, one can write:

$$p = f_{\text{non}\,b}\, S_F^{\text{non}\,b}\, p_{\text{non}\,b} + (1 - f_{\text{non}\,b}\, S_F^{\text{non}\,b}) \times \\ \times \left(p_{\text{pair}}\, p_{J_Q}\, S_F^{J_Q} + (1 - p_{\text{pair}})(1 - p_{J_Q}\, S_F^{J_Q}) \right). \quad (9)$$

The combined purity should be calculated for the signal process as well as for the background processes. Note that for the SM scenario it is expected that the purity is more than 50% ($p > 0.5$), while for the background it should be around 50% ($p \approx 0.5$). In data, the combined purity less than 50% will give preference to the XM scenario.

To find purity for the background, all important background processes in both channels were taken into account. In the LJ channel, the main background processes are: $W+$jets production (the most significant background), $Z+$jets, QCD multijets, diboson and single top-quark production. In the DL channel, the dominant background is from $W+$multijet events where one of jets is misidentified as lepton and one of jets as a b jet. The other backgrounds are Drell–Yan $+$ jets, where there is an instrumental missing E_T and a jet misidentified as a b jet, and diboson production.

An important issue at the estimate of the background is determination of systematic uncertainties. In this analysis the systematic uncertainties include effects of the parton distribution functions (PDFs), initial and final state radiation (ISR and FSR), jet energy scale, choice of MC generator, uncertainties on the background predictions and the uncertainty on the luminosity. These uncertainties are estimated by comparing different choices of PDFs, by varying ISR, FSR and the jet energy scale in MC, by comparing PYTHIA and HERWIG, etc.

Table 7. **The expected background and signal purities for an integrated luminosity of 1.5 fb^{-1}. N_b is the number of events that passed the selection criteria, N^+ (N^-) is the number of SM (XM)-like pairs**

Channels	N_b or N_s	Purity	N^+	N^-
LJ/background	3.15±0.99	$0.503^{+0.002}_{-0.002}$	1.59±0.50	1.57±0.49
LJ/signal	72.09±12.73	$0.569^{+0.004(\text{stat.})}_{-0.010(\text{syst.})}$	41.02±7.28	31.07±5.54
DL/background	$0.96^{+1.47}_{-0.73}$	$0.513^{+0.016}_{-0.014}$	$0.49^{+0.76}_{-0.38}$	$0.47^{+0.71}_{-0.35}$
DL/signal	13.44±1.60	$0.587^{+0.006(\text{stat.})}_{-0.013(\text{syst.})}$	7.89±0.96	5.55±0.69
Total background	$4.11^{+1.77}_{-1.23}$	$0.505^{+0.005}_{-0.005}$	$2.08^{+0.91}_{-0.63}$	$2.04^{+0.86}_{-0.61}$
Total signal	85.54±12.83	$0.572^{+0.003(\text{stat.})}_{-0.008(\text{syst.})}$	48.91±7.35	36.62±5.58

The expected signal and backgrounds, along with the purities and expected number of SM-like (N^+) and XM-like (N^-) events are summarized in Table 7 for an integrated luminosity of 1.5 fb^{-1}.

From Table 7 it follows that in both channels the purity for the background is compatible with 0.5, while for the SM signal it is clearly bigger than 0.5. It means that in the background case no preference is given to the SM or to the XM.

Table 8. **The expected number of signal and background ℓb pairs with corresponding purities for an integrated luminosity of 1.5 fb^{-1}**

N_s	171.1±25.7
N_b	8.2±3.6
p_s	$0.572 \pm 0.003(\text{stat.}) \pm 0.008(\text{syst.})$
p_b	0.505±0.005

The expected number of events can be easily converted to the number of pairs. Since each event contains 2 top quarks (or exotic quarks) the number of ℓb pairs is obtained from the signal and background expectations multiplying them by 2. The final estimates are shown in Table 8.

2.6. Statistical Treatment. Applying the pairing and jet charge selection on experimental data, each data ℓb pair can be labeled as being SM-like or XM-like. To obtain a confidence level on either hypothesis it was assumed that both hypotheses, the SM one and XM one, can occur in parallel, and a profile likelihood method was used [52] to retrieve the confidence level. The likelihood is expressed in terms of the nuisance (N_s, N_b, p_s and p_b) and quantity f_+ defined as the fraction of signal SM ℓb pairs in a sample. It contains a Poisson term representing observed signal and 4 Gaussian terms corresponding to the nuisance parameter. Concerning the nuisance-parameter Gaussians, their mean values and standard deviations are taken from Table 8. The signal term reads:

$$L_s(x^+, x^-) = \frac{(\bar{N}_+)^{x^+} \mathrm{e}^{-\bar{N}_+}}{x^+!} \; \frac{(\bar{N}_-)^{x^-} \mathrm{e}^{-\bar{N}_-}}{x^-!}, \tag{10}$$

where $\bar{N}_+(\bar{N}_-)$ is the mean number of lb pairs of SM-like (XM-like) for an investigated sample, x^+ (x^-) is a concrete realization of the number of SM-like (XM-like) ℓb pairs for the assumed sample. The term $L_s\,(x^+, x^-)$ is a probability that random variable (x^+, x^-) will occur in experiment at the assumed integrated luminosity. The mean numbers $\bar{N}_+$ and $\bar{N}_-$ can be expressed through the nuisance parameters as follows:

$$\bar{N}_+ = p_s N_s f_+ + (1 - p_s) N_s (1 - f_+) + p_b N_b, \tag{11}$$

$$\bar{N}_- = (1 - p_s) N_s f_+ + p_s N_s (1 - f_+) + (1 - p_b) N_b. \tag{12}$$

The full likelihood L is a product of the signal term L_s and 4 Gaussians describing spreads of the nuisance parameters. To distinguish between the SM and XM scenario, the quantity f_+ was taken as the test statistic of the analysis method.

Assuming the SM or XM hypothesis and applying the technique of pseudoexperiments enabled one to find, using the maximal likelihood method, the distribution of best f_+ in both scenarios. If experimental data, denote them $(x^+_{\rm obs}, x^-_{\rm obs})$, are available, then optimization of the full likelihood $L(x^+_{\rm obs}, x^-_{\rm obs};\ f_+, N_s, N_b, p_s, p_b)$ over the space of the nuisance parameters enables to retrieve the value of f_+ as a value at the minimum of $-2\ln(L)$. Using the retrieved f_+, and the distribution of f_+ for the SM and XM scenarios, the corresponding p values can be found for both scenarios. To compare two hypotheses, the so-called Bayes factor is calculated under the scheme:

$$B_F = \frac{P(x^+_{\rm obs}, x^+_{\rm obs}|f_+ = 1)}{P(x^+_{\rm obs}, x^+_{\rm obs}|f_+ = 0)}, \tag{13}$$

where $P(x^+_{\rm obs}, x^-_{\rm obs}|f_+ = a) = \int L(x^+_{\rm obs}, x^-_{\rm obs};\ f_+ = a, N_s, N_b,\ p_s,\ p_b)\, dN_s \times dN_b dp_s\, dp_b$ is an integrated likelihood through the space of nuisance parameters for the hypothesis $f_+ = a$.

2.7. Results. The top-quark charge analysis was performed on a sample of an integrated luminosity of 1.5 fb^{-1}. The obtained results on the number of events and ℓb pairs after applying the lepton b-jet pairing and jet charge selection as well as the number of SM-like and XM-like ℓb pairs are shown in Table 9.

Table 9. **The observed number of events before ($N_{\rm obs}$) and after the ℓb pairing ($N_{\rm ev}$), the observed number of ℓb pairs with the jet charge defined ($N_{\rm pairs}$), the observed number of SM-like ($x^-_{\rm obs}$) and XM-like ($x^-_{\rm obs}$) ℓb pairs**

Yield	$N_{\rm obs}$	$N_{\rm ev}$	$N_{\rm pairs}$	$x^+_{\rm obs}$	$x^-_{\rm obs}$
$L+J$	193	102	199	111	88
Dilepton	44	14	26	13	13
Total	237	116	225	124	101

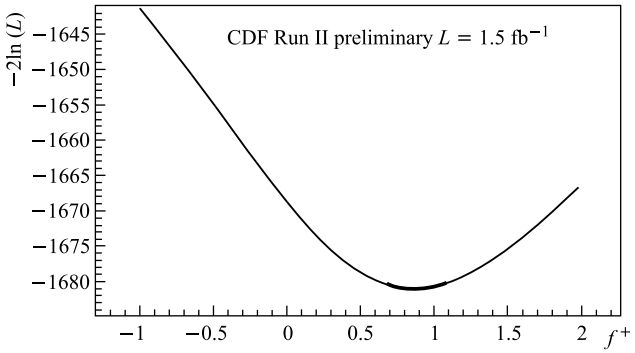

Fig. 10. Curve $-2\ln(L)$; $f_+ = 0.87$

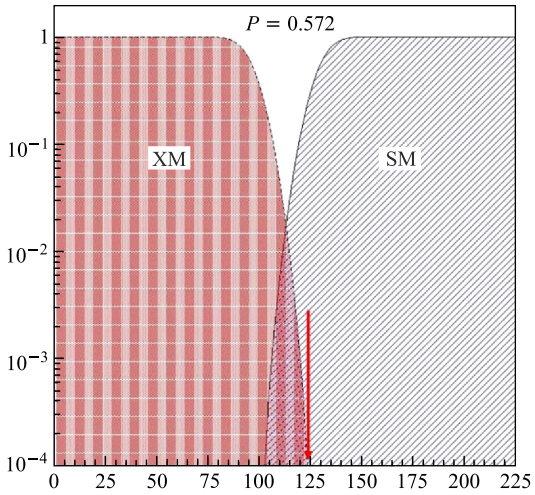

Fig. 11. The probability to occur for both the SM and the XM with the observed total number of ℓb pairs of 225 (124 indicating the SM and 101 the XM) assuming the combined probability $P = 0.572$

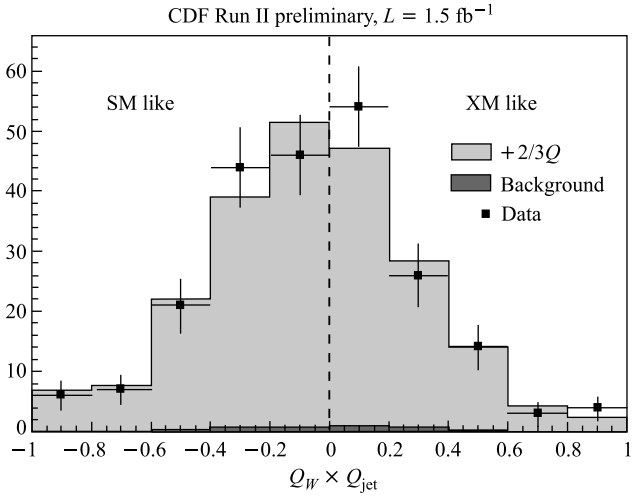

Fig. 12. Product of the W charge and the associated jet charge for data and MC («$+2/3Q$» corresponds to the SM signal MC distribution for $Q_W \times Q_{\text{jet}}$). A negative value corresponds to a SM-like pair

From the minimum of the $-2\ln(L)$ curve, for the observed numbers of ℓb pairs $(x^+_{\text{obs}}, x^-_{\text{obs}})$ a value of $f_+ = 0.87$ was retrieved (see Fig. 10). This corresponds to a p value of 0.31 for the SM using hypothesis. The corresponding Bayes factor was also calculated giving a value of $2\ln(B_F) = 12$. This value says

that the experimental data very strongly favors the SM over the XM hypothesis. In Fig. 11 is shown the probability for both the SM scenario and the XM one to occur with the observed number in total of 225 ℓb pairs (124 SM-like and 101 XM-like). The plot assumes the expected combined purity of $P_{\rm comb} = 0.572$.

A good agreement between the SM prediction and the data is demonstrated in Fig. 12 [51], where a distribution of product of the W boson charge and the associated b jet charge ($Q_W \times Q_{\rm jet}$) for the experimental data and SM Monte Carlo for the signal and background is shown.

3. SEARCH FOR $t\bar{t}$ RESONANT PRODUCTION

Resonant top-pair production in hadronic collisions has been discussed in the context of extended gauge theories with massive Z-like bosons [53–55], in theories with top-color [56], or with axigluons [57]. Decays to $t\bar{t}$ are of special interest in leptophobic models that would evade detection in traditional searches based on dielectron or dimuon signatures. More recently, resonant top pairs have been suggested as signatures for Kaluza–Klein (KK) states of gluons, weak bosons, and gravitons [58–60]; in some of these models the KK excitation couples strongly to the top quark, and $t\bar{t}$ is the dominant decay mode.

A $t\bar{t}$ resonance would appear as unexpected structure in the spectrum of the invariant mass of $t\bar{t}$ pairs $M_{t\bar{t}}$. Previous searches using ≈ 100 pb^{-1} samples from Fermilab Tevatron Run I have ruled out the production of a narrow leptophobic top-color resonance with the mass less than 480 GeV/c^2 [61, 62].

Below, in the new experiment for fully reconstructed candidate $t\bar{t}$ events triggered on leptons with large transverse momentum and containing at least one identified b-quark jet, the authors compare the invariant mass spectrum of $t\bar{t}$ pairs to the expected superposition of standard model $t\bar{t}$, non-$t\bar{t}$ backgrounds, and a simple resonance model based on a sequential Z' boson. There were established upper limits for $\sigma(p\bar{p} \to Z') \cdot {\rm Br}\,(Z' \to t\bar{t})$ in the Z' mass interval from 450 to 900 GeV/c^2. A top-color leptophobic Z' is ruled out below 720 GeV/c^2, and the cross section of any narrow Z'-like state decaying to $t\bar{t}$ is found to be less than 0.64 pb at 95% CL for $M_{Z'}$ above 700 GeV/c^2.

Limits on the Production of Narrow $t\bar{t}$ Resonances in $p\bar{p}$ Collisions at Run II. Here, [63], the authors search for resonant structure in the $M_{t\bar{t}}$ spectrum in 955 pb^{-1} of $p\bar{p}$ collisions at $\sqrt{s} = 1.96$ TeV recorded with the CDF II detector. Modeling the resonance as a narrow massive vector boson $\mathbf{Z}'$, and calculating its mass with techniques used in precision measurement of the top-quark mass [13], there were set limits on the cross section times branching ratio $\sigma B = \sigma(p\bar{p} \to \mathbf{Z}') \cdot {\rm Br}\,(Z' \to t\bar{t})$ as a function of $M_{Z'}$. This study is complementary to [64], which uses a different event selection and reconstruction of the $t\bar{t}$ kinematics.

CDF II detector [29, 41] provides precision track reconstruction. The data used here were recorded between March 2002 and January 2006.

The authors collect a sample of $t\bar{t} \to W^+bW^-\bar{b}$ candidate events with one leptonic W-boson decay using triggers that require a central ($|\eta| \leqslant 1.0$) electron with $E_T > 18$ GeV or central muon with transverse momentum $p_T > 18$ GeV/c. After offline reconstruction, there were selected events with an isolated electron with $E_T \geqslant 20$ GeV or muon with $p_T \geqslant 20$ GeV/c, missing transverse energy $\not\!\!E_T \geqslant 20$ GeV consistent with a neutrino from W decay, and at least four hadronic jets with $|\eta| \leqslant 2.0$ of which three must have $E_T \geqslant 15$ GeV, and the fourth must have $E_T \geqslant 8$ GeV. The jets are clustered in fixed cones of radius $\Delta R = \sqrt{(\Delta\eta)^2 + (\Delta\varphi)^2} \leqslant 0.4$. At least one of the jets is required to be b-tagged, i.e., to contain a reconstructed secondary vertex displaced from the primary event vertex as expected from the decay of a bottom hadron in the jet [41]. The authors find 347 events fulfilling these criteria.

The sample is dominated by s-channel $q\bar{q}$ annihilation into $t\bar{t}$ pairs [24, 26]. The $t\bar{t}$ acceptance and efficiencies are calculated using the HERWIG generator [21] and a detector simulation, assuming a top mass $M_t = 175$ GeV/c^2. The simulated detector response, particularly with respect to lepton isolation, jet energies, and b-tagging, has been tuned in an earlier measurement of the top pair production cross section [19]. The total combined trigger and reconstruction efficiency is $(3.5 \pm 0.5)\%$. Non-$t\bar{t}$ backgrounds include W bosons produced in association with jets ($W+$jets), where a light flavor jet is incorrectly b-tagged; $W+$jet events with real heavy-flavor jets; mismeasured QCD multijet events with one jet identified as a lepton; and smaller contributions from electroweak processes such as diboson (WW, WZ, ZZ) and single-top production. The rates and kinematics of these processes are modeled with simulated and data control samples as employed in the top cross section measurement [19]. A total of (73 ± 9) non-$t\bar{t}$ background events are expected.

The final state of four jets, a high-p_T lepton, and E_T allow an overconstrained (2C) reconstruction of the top pair kinematics. The assignment of jets to quarks most consistent with the $t\bar{t}$ hypothesis is determined using the χ^2 minimization algorithm employed in the measurement of the top mass [13]. Here, following [37], we include the known top mass as a constraint, which improves the accuracy of the parton assignments. The measured jet energies are corrected back to parton values using calibrations derived from photon-jet balancing and detector simulation [18]. In the χ^2 minimization the parton energies are varied within their uncertainties and the W and top masses are constrained to the values $M_W = 80.4$ GeV/c^2 and $M_t = 175.0$ GeV/c^2 within their natural widths (2.1 and 1.5 GeV/c^2, respectively). The effect of variation in the central value of M_t is included later as a systematic uncertainty. Jets with b tags must be associated with b quarks. The jet-quark assignment giving the lowest χ^2 consistent

with these constraints is chosen as the solution. In simulated $t\bar{t}$ events we find a small number of poorly reconstructed events flagged by extreme χ^2. The authors find that the sensitivity of the search is optimized by requiring $\chi^2 < 50$; this cut removes 4% of $t\bar{t}$ events and 9% of non-$t\bar{t}$ backgrounds.

The authors model the resonant $t\bar{t}$-production mechanism as a sequential Z', a heavy neutral boson with the same couplings as the Z, here including decay to $t\bar{t}$ with $M_t = 175$ GeV/c^2. This color-singlet resonance has no interference with the standard color-octet $t\bar{t}$ production processes and the model lineshape is purely Lorentzian. To facilitate comparison to other results [9, 10, 64] we assign the same narrow width used there, $\Gamma_{Z'} = 0.012 M_{Z'}$. A strictly sequential Z' with open $t\bar{t}$ decays has $\Gamma_{Z'} = 0.03 M_{Z'}$. Since our reconstructed mass resolution is greater than 60 GeV$/c^2$ (see below) the analysis is insensitive to model dependent width differences at this level, and applies to any narrow $t\bar{t}$ state appearing as a single enhancement in the $M_{t\bar{t}}$ spectrum. Signal models are generated using the PYTHIA simulation [20] with Z' masses between 450 and 900 GeV$/c^2$ in increments of 50 GeV$/c^2$.

The inset of Fig. 13 shows the $M_{t\bar{t}}$ distribution reconstructed for a simulated 750 GeV$/c^2$ Z'. There is a peak near the expected value and a low mass tail

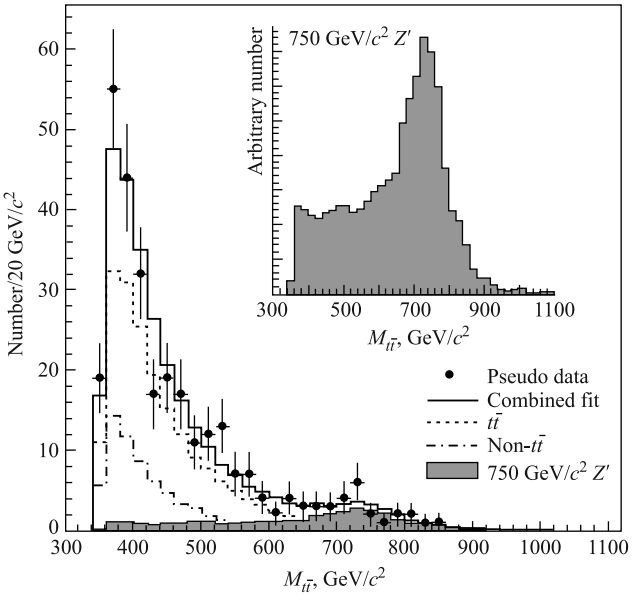

Fig. 13. Simulated $M_{t\bar{t}}$ spectrum for 955 pb^{-1} in presence of a 750 GeV/c^2 Z' with $\sigma B = 1$ pb (shaded area). The points are a simulated data set. The solid line is the best fit to a superposition of the Z' signal (solid histogram) and the expected $t\bar{t}$ (dotted line) and non-$t\bar{t}$ (dash-dotted line) backgrounds. The inset shows the reconstructed $M_{t\bar{t}}$ spectrum in an arbitrarily large sample of simulated 750 GeV/c^2 Z'. The low mass tail arises from incorrect jet-parton associations

which arises from the incorrect jet-parton assignments where a jet from initial or final state radiation has been used instead of a jet from top decay. The rms of the peak region is approximately 60 GeV/c^2 and the full rms is 137 GeV/c^2. Other Z' masses show similar behavior: the $M_{Z'}$ peak width is preserved and the low mass tail extends down to the kinematic threshold at 350 GeV/c^2. The full rms of the $M_{t\bar{t}}$ distribution varies between 67 and 178 GeV/c^2 over our Z' mass range. The fraction of Z' removed by the χ^2 cut varies between 4 and 9% over the Z' mass range.

There was used a three-parameter binned likelihood maximization to fit the $M_{t\bar{t}}$ spectrum to a superposition of the expected shapes for $Z' \to t\bar{t}$ standard model $t\bar{t}$, and non-$t\bar{t}$ processes. In the ith bin, we expect

$$\mu_i = \left[\sigma B A \varepsilon \int L\, dt\right] P_{z|,i}, + N_{t\bar{t}} P_{t\bar{t},i} + N_{\mathrm{bkg}} P_{\mathrm{bkg},i}, \tag{14}$$

where P'_z, i, $P_{t\bar{t},i}$, and $P_{\mathrm{bkg},i}$ are the probabilities of observing a signal event, event or non-$t\bar{t}$ background event in bin i, respectively. $N_{t\bar{t}}$ and N_{bkg} are the number of non-resonant $t\bar{t}$ and the non-$t\bar{t}$ background events. The $\sigma B A \varepsilon \int L\, dt$ term contains the product of cross section and $t\bar{t}$ branching ratio, acceptance, and efficiency for the Z', and the luminosity.

A likelihood function L for the distribution can be written as

$$L = \prod P_i(n_i|\mu_i)\, G\,(\nu_k|\bar{v}_k, \sigma\bar{v}_k). \tag{15}$$

The function $P_i(n_i|\mu_i)$ is the Poisson probability for observing n_i events in a bin i, where μ_i are expected. The functions $G(v_k|\bar{\nu}_k, \sigma_{\nu_k})$ constrain the nuisance parameters v_k, which include the non-$t\bar{t}$ background normalization N_{bkg}, b-tag efficiency, acceptances and luminosities, with Gaussian probability around their central values $\bar{\nu}_k$ and uncertainties σ_{ν_k}. The $t\bar{t}$ and non-$t\bar{t}$ background values are taken from [19], and the Z' acceptances and efficiencies are determined from the PYTHIA simulation. There were found $\sigma B, N_{t\bar{t}}, N_{\mathrm{bkg}}$, and v_k that maximize the likelihood function for each $M_{Z'}$.

The algorithm is tested with simulated samples, where the $t\bar{t}$, non-$t\bar{t}$, and Z' models are combined in the expected ratios and sampled with the expected level of statistical fluctuations. The points in the main part of Fig. 13 show the $M_{t\bar{t}}$ distribution for a simulated data sample corresponding to an integrated luminosity of 955 pb^{-1} in the case of a 750 GeV/c^2 Z' with $\sigma B = 1$ pb. The histograms show the components as resolved by the likelihood fit. The extraction of the Z' component uses shape information from the low mass part of the spectrum as well as the peak area.

The 95% CL upper limit on σB at a given mass is found by integrating the likelihood along σB, reoptimizing at each point, to find the value that

contains 95% of the area. The expected sensitivity was measured using large ensembles of simulated samples like the one shown in Fig. 13. The main sources of systematic uncertainty are the acceptance change due to energy scale uncertainty on the jet thresholds, and the shape change in $M_{t\bar{t}}$ from the top mass uncertainty of 3 GeV/c^2. Model-dependent shape effects associated with initial and final state gluon radiation and non-$t\bar{t}$ backgrounds are small. PDF uncertainties are evaluated using simulated samples generated with MRST [65] and the full set of eigenvectors from CTEQ6M [66]. Simulated samples with reasonable variations for systematic effects are used to measure the apparent shifts in the fitted σB as a function of the true value. The sum of the shifts in quadrature is used as the width of a Gaussian resolution function that is convolved with the likelihood as a function of σB. The systematic uncertainties worsen the limits by roughly 0.2 pb, independent of the Z' mass, with the increase dominated by the effects of jet energy scale and the top mass uncertainty in equal measure. The expected 95% CL upper limits including all sources of uncertainty are shown as a function of $M_{Z'}$ in the middle column of Table 10.

The $M_{t\bar{t}}$ distribution measured in the data is shown in Fig. 14. A final sample of 327 candidates remains after the χ^2 requirement. In this figure the observation is compared to the expected spectrum in the case of no Z'. The non-$t\bar{t}$ component is fixed at the expected value and the $t\bar{t}$ normalization is scaled to match the total number of events. The inferred top production cross section is $\sigma(t\bar{t}) = (7.8 \pm 0.7)$ pb (statistical error only), to be compared with the predicted

Table 10. **Expected and observed limits (95% CL) on $\sigma(p\bar{p} \to Z') \cdot \mathrm{Br}\,(Z' \to t\bar{t})$ as a function of $M_{Z'}$ for 955 pb^{-1}, including both statistical and systematic uncertainties**

$M_{Z'}$, GeV/c^2	Expected limit, pb	Observed limit, pb
450	$2.27^{+0.79}_{-0.57}$	3.39
500	$1.92^{+0.63}_{-0.40}$	2.72
550	$1.37^{+0.45}_{-0.30}$	1.57
600	$0.97^{+0.33}_{-0.18}$	0.83
650	$0.78^{+0.24}_{-0.13}$	0.65
700	$0.70^{+0.14}_{-0.12}$	0.64
750	$0.64^{+0.15}_{-0.11}$	0.61
800	$0.58^{+0.15}_{-0.07}$	0.60
850	$0.55^{+0.10}_{-0.05}$	0.57
900	$0.55^{+0.08}_{-0.06}$	0.57

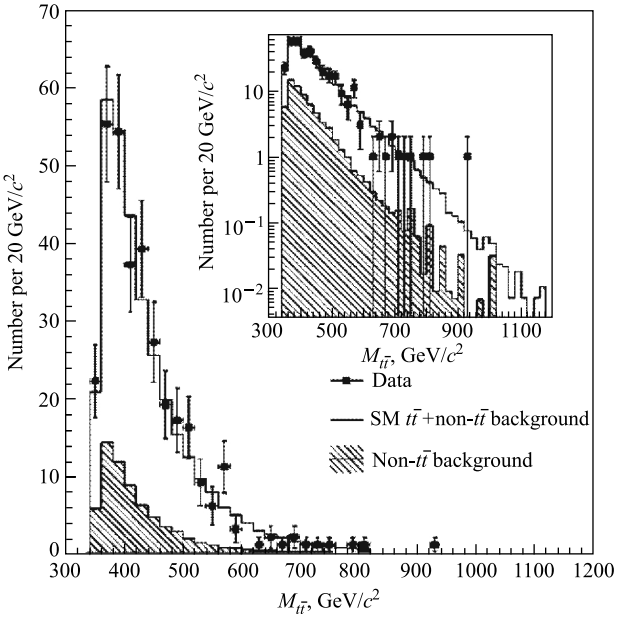

Fig. 14. The invariant mass of top-quark pairs $M_{t\bar{t}}$ observed in the data is compared to the no Z' expectation. The non-$t\bar{t}$ backgrounds are constrained to the expected value and the sum of $t\bar{t}$ and non-$t\bar{t}$ equals the number of data events

standard model value of 6.7 pb for $M_t = 175$ GeV/c^2 [24, 26]. The inset shows the measurement on a logarithmic scale. The simulated $M_{t\bar{t}}$ spectra for $t\bar{t}$ and non-$t\bar{t}$ describe the data well.

Applying the full limit procedure to the spectrum in Fig. 14 we find 95% CL upper limits on $\sigma(p\bar{p} \to Z') \cdot \mathrm{Br}\,(Z' \to t\bar{t})$ as listed in the rightmost column of Table 10. The limits at high mass are consistent with expectation. At lower masses our measurement shows an excursion above the expected value of approximately 1 standard deviation.

The result is represented graphically and compared to some theoretical predictions in Fig. 15. The observed limit is the solid black line and the shaded band around the gray line denotes the $\pm 1\sigma$ uncertainties around the expected upper limit. A leptophobic Z' predicted by the top color theory [56], shown as a large-dotted line, is ruled out below 720 GeV$/c^2$ at 95% CL. The small-dotted curve at the bottom of the figure is the expected cross section for a sequential Z', calculated with the HERWIG simulation using a multiplicative factor of 1.3 to account for NLO effects.

A leptophobic Z' with these couplings would evade direct searches in dilepton final states, and because the $t\bar{t}$ detection efficiency is small, it is still out of range

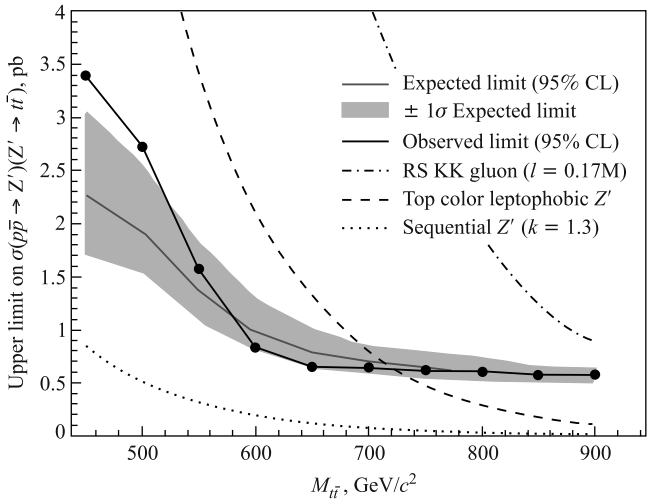

Fig. 15. Upper limits (95% CL) on the production cross section for $t\bar{t}$ resonance along with expected cross sections for several models

of our sensitivity in the $t\bar{t}$ mode. The Tevatron cross section for the KK gluon excitation in the Randall–Sundrum model of [58] is shown as a dash-dotted line [67, 68]. Since the KK resonance is broad ($\Gamma \sim 0.17M$), and the limits derived in the «narrow width» assumption are not strictly applicable, authors show the curve here for qualitative comparison. The cross section of any narrow Z'-like state produced in $p\bar{p}$ collisions at $\sqrt{s} = 1.96$ TeV and subsequently decaying to $t\bar{t}$ is less than or equal to 0.64 pb (95% CL) for all M'_Z above 600 GeV/c^2.

Acknowledgements. We would like to thank very much associated Professor S. Tokar for reading the draft of this article and for very precious comments and additions; A. V. Sazonova and doctor D. Sh. Chokhely for great technical help and programming service.

REFERENCES

1. *Abe F. et al. (CDF Collab.).* Observation of Top Quark Production in $\bar{p}p$ Collisions with the Collider Detector at Fermilab // Phys. Rev. Lett. 1995. V. 74. P. 2626.
2. *Abachi S. et al. (DØ Collab.).* Observation of the Top Quark // Ibid. P. 2632.
3. *Abulencia A. et al.* Measurement of the Helicity Fractions of W Bosons from Top Quark Decays Using Fully Reconstructed $t\bar{t}$ Events with CDF II // Phys. Rev. D. 2007. V. 75. P. 052001.

4. *Aaltonen T. (CDF Collab.).* Measurement of W-Boson Helicity Fractions in Top-Quark Decays Using $\cos\theta^*$ (Quoted in this Article) // Phys. Lett. B. 2009. V. 674. P. 160;
Fischer M. et al. Longitudinal, Transverse-Plus and Transverse-Minus W Bosons in Unpolarized Top Quark Decays at $O(\alpha_s)$ // Phys. Rev. D. 2001. V. 63. P. 031501(R);
Do H. S. et al. Electroweak and Finite Width Corrections to Top Quark Decays into Transverse and Longitudinal W Bosons // Phys. Rev. D. 2003. V. 67. P. 091501(R).

5. *Lee T. D., Yang C. N.* Parity Nonconservation and a Two-Component Theory of the Neutrino // Phys. Rev. 1957. V. 105. P. 1671;
Landau L. On the Conservation Laws for Weak Interactions // Nucl. Phys. 1957. V. 3. P. 127;
Salam A. On Parity Conservation and Neutrino Mass // Nuovo Cim. Ser. 10. 1957. V. 5. P. 299–301;
Feynman R. P., Gell-Mann M. Theory of the Fermi Interaction // Phys. Rev. 1958. V. 109. P. 193;
Sudarshan E. C. G., Marshak R. E. Chirality Invariance and the Universal Fermi Interaction // Phys. Rev. 1958. V. 109. P. 1860.

6. *Tevatron Electroweak Working Group.* A Combination of CDF and DØ Results on the Mass of the Top Quark. arXiv:0808.1089 [hep-ex]. B33.

7. *Peccei R. D., Zhang X.* Dynamical Symmetry Breaking and Universality Breakdown // Nucl. Phys. B. 1990. V. 7. P. 269.

8. *Yao W. M. et al.* Review of Particle Physics. The 2006 Edition Is Published for the Particle Data // J. Phys. G. 2006. V. 33. P. 1.

9. *Kane G. L., Ladinsky G. A., Yuan C. P.* Using the Top Quark for Testing Standard-Model Polarization and *CP* Predictions // Phys. Rev. D. 1992. V. 45. P. 124.

10. *Fischer M. et al.* Longitudinal, Transverse-Plus and Transverse-Minus W Bosons in Unpolarized Top Quark Decays at $O(\alpha_s)$ // Phys. Rev. D. 2001. V. 63. P. 031501(R).

11. *Acosta D. et al. (CDF Collab.).* Measurement of the W Boson Polarization in Top Decay at CDF $\sqrt{s} = 1.8$ TeV // Phys. Rev. D. 2005. V. 71. P. 031101.

12. *Jezabek A., Kuhn J. H.* // Nucl. Phys. B. 1989. V. 314. P. 1; Semileptonic Decays of Top Quarks // Phys. Lett. B. 1988. V. 207. P. 91;
Czarnecki A., Melnikov K. Two-Loop QCD Corrections to Top Quark Width // Nucl. Phys. B. 1999. V. 544. P. 520;
Chetyrkin K. G. et al. Second order QCD Corrections to $\Gamma(t \to Wb)$ // Phys. Rev. D. 1999. V. 60. P. 114015.

13. *Abulencia et al. (CDF Collab.).* Top Quark Mass Measurement Using the Template Method in the Lepton + Jets Channel at CDF II // Phys. Rev. D. 2006. V. 73. P. 032003.

14. *Hirschbuehl D.* Ph.D. Thesis. University of Karlsruhe. FERMILAB-THESIS-2005-80. 2005.

15. *Chwalek Th.* Diploma Thesis. University of Karlsruhe. FERMILAB-MASTERS-2006-04. 2006.

16. *Aaltonen T. et al. (CDF Collab.)*. Forward-Backward Asymmetry in Top-Quark Production in $p\bar{p}$ Collisions at $\sqrt{s} = 1.96$ TeV // Phys. Rev. Lett. 2008. V. 101. P. 202001.

17. *Abazov V. M. et al. (DØ Collab.)*. Model-Independent Measurement of the W-Boson Helicity in Top-Quark Decays at DØ // Ibid. V. 100. P. 062004.

18. *Bhatti A. et al. (CDF Collab.)*. Determination of Jet Energy Scale at CDF // Nucl. Instr. Meth. A. 2006. V. 566. P. 375; Phys. Rev. D. 2010. V. 81. P. 052006.

19. *Abulencia A. et al. (CDF Collab.)*. Measurement of the $t\bar{t}$ Production Cross Section in $p\bar{p}$ Collisions at $\sqrt{s} = 1.96$ TeV // Phys. Rev. Lett. 2006. V. 97. P. 082004.

20. *Sjostrand T. et al.* PYTHIA 6.2 Physics and Manual // Comp. Phys. Commun. 2001. V. 135. P. 238; hep-ph/0108264.

21. *Corcella G. et al.* An Event Generator for Hadron Emission Reactions with Interfering Gluons (Including Supersymmetric Processes). hep-ph/0011363; hep-ph/0210213; HERWIG // J. High Energy Phys. 2001. V. 01. P. 010.

22. *Mangano M. L. et al. (ALPGEN)*. A Generator for Hard Multiparton Processes in Hadronic Collisions // J. High Energy Phys. 2003. V. 0307. P. 001.

23. *Event Jd.* V4: The New Web Generation // J. High Energy Phys. 2007. V. 0709. P. 028.

24. *Affolder T. et al.* CDF Run II Silicon Tracking Projects // Nucl. Instr. Meth. A. 2000. V. 447. P. 1;
Kidonakis N., Vogt R. Next-to-Next-to-Leading Order Soft-Gluon Corrections in Top Quark Adroproduction // Phys. Rev. D. 2003. V. 68. P. 114014.

25. *Moed S.* Ph.D. Thesis. University of Geneua. FERMILAB-THESIS-2007-70.

26. *Cacciari M. et al.* The $t\bar{t}$ Cross-Section at 1.8 and 1.96 TeV: A Study of the Systematics due to Parton Densities and Scale Dependence // J. High Energy Phys. 2004. V. 404. P. 068.

27. *Lyons L., Gibaut D., Clifford P.* How to Combine Correlated Estimates of a Single Physical Quantity // Nucl. Instr. Meth. A. 1988. V. 270. P. 110;
Valassi A. Combining Correlated Measurements of Several Different Physical Quantities // Nucl. Insrt. Meth. A. 2003. V. 500. P. 391.

28. *CDF Collab.* Measurement of W Boson Helicity Fractions in Top Decay to Lepton + Jets Using Matrix Element // CDF Conf. 2008.

29. The CDF II Detector Technical Design Report. Fermilab-Pub-96/390-E;
LeCompte T., Diehl H. T. The CDF and DØ Upgrades for Run II // Annu. Rev. Nucl. Part. 2000. V. 50 P. 71–117; Technique in 1.9 fb^{-1} Data // 2007. Conf. Note. 9144.

30. *Abulencia A. et al. (CDF Collab.)*. Search for $V + A$ Current in Top-Quark Decays in $p\bar{p}$ Collisions at $\sqrt{s} = 1.96$ TeV // Phys. Rev. Lett. 2007. V. 98. P. 072001.

31. *Jezabek M., Kuhn J. H.* QCD Corrections to Semileptonic Decays of Heavy Quarks // Nucl. Phys. B. 1989. V. 314. P. 1.

32. *Fischer M. et al.* Longitudinal, Transverse-Plus and Transverse-Minus W Bosons in Unpolarized Top Quark Decays at $O(\alpha_s)$ // Phys. Rev. D. 2001. V. 63. P. 031501(R).

33. *Do H. S. et al.* Electroweak and Finite Width Corrections to Top Quark Decays into Transverse and Longitudinal W Bosons // Phys. Rev. D. 2003. V. 67. P. 091501(R).

34. *Beg M. A. B. et al.* Manifest Left-Right Symmetry and Its Experimental Consequences // Phys. Rev. Lett. 1977. V. 38. P. 1252.

35. *Triantaphyllou G.* New Physics with Mirror Particles // J. Phys. G. 2000. V. 26. P. 99.

36. *Choudhury D., Tait T. M. P., Wagner C. E. M.* Beautiful Mirrors and Precision Electroweak Data // Phys. Rev. D. 2002. V. 65. P. 053002.

37. *Abulencia A. et al. (CDF Collab.).* Measurement of the Helicity of W Bosons in Top-Quark Decays // Phys. Rev. D. 2006. V. 73. P. 111103.

38. *Abazov V. M. et al. (DØ Collab.).* Helicity of the W Boson in Lepton + Jets in $t\bar{t}$ Events // Phys. Lett. B. 2005. V. 617. P. 1.

39. *Abazov V. M. et al. (DØ Collab.).* Search for Right-Handed W Bosons in Top Quark Decay // Phys. Rev. D. 2005. V. 72. P. 011104(R).

40. *Larios F., Perez M. A., Yuan C. P.* Analysis of $t - b - W$ and $t - t - Z$ Couplings from CLEO and EP/SLC Data // Phys. Lett. B. 1999. V. 457. P. 334.

41. *Acosta D. et al. (CDF Collab.).* Measurement of the J/ψ Meson and b-Hadron Production Cross Sections in $p\bar{p}$ Collisions at $\sqrt{s} = 1960$ GeV // Phys. Rev. D. 2005. V. 71. P. 052003;
Flyagin V. et al. The Top-quark, Other New Phenomena Observed at the CDF in $p\bar{p}$ Collision at $\sqrt{s} = 1.96$ TeV // Part. Nucl. 2010. V. 41, No. 3. P. 661–719.

42. *Lai H. L. et al. (CTEQ Collab.).* Global QCD Analysis of Parton Structure of the Nucleon: CTEQ5 Parton Distributions // Eur. Phys. J. C. 2000. V. 12. P. 75.

43. *Gerchtein E., Paulini M.* // Proc. of 2003 Conf. for Computing in High-Energy and 20 Nuclear Physics (CHEP 03), CHEP, La Jolla, CA, USA, California. 2003). Conf C0303241. TUMT005.

44. *Brun R. et al.* CERN Report No. CERN-DD/EE/84-1. 1987.

45. *Acosta D. et al. (CDF Collab.).* Measurement of the $t\bar{t}$ Production Cross section in $p\bar{p}$ Collisions at $\sqrt{s} = 1.96$ TeV Using Dilepton Events // Phys. Rev. Lett. 2004. V. 93. P. 142001.

46. *Chang D., Chang W. F., Ma E.* Alternative $(-4/3)$ Interpretation of the Fermi Tevatron Top Events // Phys. Rev. D. 1999. V. 59. P. 091503.

47. *Baur U., Buice M., Orr L. H.* Direct Measurement of the Top Quark Charge at Hadron Colliders // Phys. Rev. D. 2001. V. 64. P. 094019.

48. *Mangano G., Altarelli M.* // Proc. of the Workshop on Standard Model Physics and the LHC. Geneva: CERN, 2000.

49. *Ciljak M.* Top Charge Measurement at ATLAS Detector. Geneva: CERN, 2003. ATL/PHYS-2003-035.

50. *Abazov A. M. et al. (DØ Collab.).* Experimental Discrimination between Charge $2e/3$ Top Quark and Charge $4e/3$ Exotic Quark Production Scenarios // Phys. Rev. Lett. 2007. V. 98. P. 041801.

51. *CDF Collab.* First CDF Measurement of the Top Quark Charge Using the Top Decay Products. CDF/PHYS/TOP/PUBLIC/8967. Conf. Note. 2007.
52. *Rolke W. A. et al.* Limits and Confidence Intervals in the Presence of Nuisance Parameters // Nucl. Instr. Meth. A. 2005. V. 551. P. 493–503; physics/0403059.
53. *Rosner J.* Prominent Decay Modes of a Leptophobic Z' // Phys. Lett. B. 1996. V. 387. P. 113.
54. *Leike A.* Searches for New Physics in the Top Quark Samples at CDF // Phys. Rep. 1999. V. 317. P. 143.
55. *Carena M. et al.* Z^0 Gauge Bosons at the Fermilab Tevatron // Phys. Rev. D. 2004. V. 70. P. 093009.
56. *Hill C., Parke S.* Top Quark Production: Sensitivity to New Physics // Phys. Rev. D. 1998. V. 49. P. 4454.
57. *Sehgal L., Wanninger M.* Forward-Backward Asymmetry in Two-Jet Events: Signature of Axigluons in Proton–Antiproton Collisions // Phys. Lett. B. 1988. V. 200. P. 211.
58. *Lillie B., Randall L., Wang L. T.* The Bulk RS KK-Gluon at the LHC // J. High Energy Phys. 2007. V. 09. P. 074.
59. *Burdman Dobrescu B., Ponton E.* Resonances from Two Universal Extra Dimensions // Phys. Rev. D. 2006. V. 74. P. 075008.
60. *Fitzpatrick L. et al.* Searching for the Kaluza–Klein Graviton in Bulk RS Models // J. High Energy Phys. 2007. V. 09. P. 013.
61. *Affolder A. et al. (CDF Collab.).* Search for New Particles Decaying to $t\bar{t}$ in $p\bar{p}$ Collisions at $\sqrt{s} = 1.8$ TeV // Phys. Rev. Lett. 2000. V. 85. P. 2062.
62. *Abazov V. et al. (DØ Collab.).* Search for Narrow $t\bar{t}$ Resonances in $p\bar{p}$ Collisions at $\sqrt{s} = 1.8$ TeV // Phys. Rev. Lett. 2004. V. 92. P. 221801.
63. *Aaltonen T. (CDF Collab.).* Limits on the Production of Narrow $t\bar{t}$ Resonances in $p\bar{p}$ Collisions at $\sqrt{s} = 1.96$ TeV // Phys. Rev. D. 2008. V. 77. P. 051102 (that we partly use as citation).
64. *Aaltonen T. et al. (CDF Collab.).* Search for Resonant $t\bar{t}$ Production in $p\bar{p}$ Collisions at $\sqrt{s} = 1.96$ TeV // Phys. Rev. Lett. 2008. V. 100. P. 231801; arXiv:0709.0705;
65. *Martin A. D. et al.* Parton Distributions and the LHC: W and Z Production // Eur. Phys. J. C. 2002. V. 14. P. 133.
66. *Pumplin J. et al.* CDF Run II Silicon Tracking Projects // Nucl. Instr. Meth. A. 2002. V. 447. P. 1.
67. The Tevatron curves were generated by Ben Lillie, based on work in [58].
68. *Aaltonen T. et al. (CDF Collab.).* Measurement of W-Boson Polarization in Top-Quark Decay in $p\bar{p}$ Collisions at $\sqrt{s} = 1.96$ TeV // Phys. Rev. Lett. 2010. V. 105. P. 042002.